Check for updates

Advanced Science

ADVANCED SCIENCE Open Access

www.advancedscience.com

RESEARCH ARTICLE OPEN ACCESS

Unsuccessful Coupling of Weakly Coordinating Anion–Based Mg Salts and Alkoxyalkylamine Solvents for Rechargeable Mg Battery Application: Trace Water-Driven Interfacial Failure

Toshihiko Mandai[1] | Antoine Barthélemy[2] | Hendrik Koger[2] | Harald Scherer[2] | Ingo Krossing[2]

[1]Research Center for Energy and Environmental Materials (GREEN), National Institute for Materials Science (NIMS), Tsukuba, Ibaraki, Japan | [2]Institute For Inorganic Chemistry and Analytic Chemistry as Well as Freiburg Materials Research Center FMF, University of Freiburg, Freiburg, Germany

Correspondence: Toshihiko Mandai (mandai.toshihiko@nims.go.jp)

Received: 30 March 2026 | **Revised:** 9 July 2026 | **Accepted:** 22 July 2026

Keywords: anion | electrolyte | interface | magnesium battery | solvation

ABSTRACT

Rechargeable magnesium metal batteries (RMMBs) are promising candidates for large-scale energy storage owing to the advantageous properties of magnesium metal negative electrodes. Recent advances, particularly in electrolyte chemistry, have accelerated progress toward practical RMMBs. Here, we combined two emerging concepts—weakly coordinating anion (WCA)-based Mg salts and alkoxyalkylamine solvents—in electrolyte design. Unexpectedly, the combination of a representative WCA-based Mg salt, $Mg[Al(Ohfip)_4]_2$, and a conventional alkoxyalkylamine, 2-methoxyethylamine (MOEA), resulted in inferior electrochemical performance, whereas MOEA favored strongly coordinating anion-based Mg salts such as $Mg[TfO]_2$. Comprehensive analyses revealed distinct anion-dependent solvation structures and interfacial chemistries. In $Mg[Al(Ohfip)_4]_2$ systems, the anion and the solvent complexes are only minimally involved in initial Mg-interface formation. Yet, the presence of trace water in MOEA induces the MOEA-mediated partial hydroxylation of the anion $[Al(Ohfip)_4]^-$, which leads to the formation of unstable oxygen-rich interfaces upon cycling. On the contrary, Mg^{2+}, $[TfO]^-$, and MOEA form associative ion-paired complexes that jointly contribute to the formation of fluorine- and nitrogen-rich hybrid interfaces that suppress parasitic reactions and enhance performance. Despite these benefits, the associative $Mg[TfO]_2$–MOEA electrolyte still exhibits limitations for practical RMMB application. The complex dilemma in developing rational electrolyte materials for RMMB applications will also be discussed.

1 | Introduction

The global demand for electricity continues to rise exponentially with advancements in science and technology. In recent years, the rapid expansion of artificial intelligence has further accelerated electricity consumption worldwide. This trend necessitates continuous innovation in energy storage technologies that harness renewable power sources such as wind and solar energy. According to market forecasts, global battery demand is expected to exceed 5000 GWh by 2040—far surpassing the available lithium capacity [1]. Therefore, the development of rechargeable batteries based on non-lithium chemistries has become increasingly imperative. Among these, rechargeable magnesium metal batteries (RMMBs) are particularly promising for large-scale energy storage applications, owing to the high 2.33% natural abundance of magnesium in the earth crust

This is an open access article under the terms of the Creative Commons Attribution License, which permits use, distribution and reproduction in any medium, provided the original work is properly cited.

© 2026 The Author(s). *Advanced Science* published by Wiley-VCH GmbH

(cf. Li: 0.006%) [2, 3]. The theoretical energy density of RMMBs can rival that of current Lithium Ion Batteries (LIBs), benefiting from the two-electron chemistry enabled by the transport of divalent Mg^{2+} ions. Moreover, the electrochemical and chemical properties of Mg metal—its low tendency to form dendrites during electroplating and the inherent stability of bulk Mg against ambient conditions—make it an attractive choice for developing safe, practical batteries.

The development and successful application of weakly coordinating anion (WCA)-based electrolytes have driven significant recent progress in the field of RMMBs [4, 5]. Certain WCA-based electrolytes have demonstrated reversible Mg plating and stripping behavior with excellent cycling efficiency, even in the absence of conventional double-edged reagents such as $[BH_4]^-$ and chloride species [6–8]. A wide range of WCAs, primarily composed of group XIII element complexes, have been investigated to date, including $[HCB_{11}H_{11}]^-$ [6, 9], $[HCB_{11}H_{10}F]^-$ [10], $[B(Otfe)_4]^-$(Otfe = OCH_2CF_3) [11, 12], $[B(Ohfip)_4)]^-$(Ohfip = $OCH(CF_3)_2$) [8, 13–16], $[B(Otfe)_3(TfO)]^-$ (TfO = OSO_2CF_3) [17], and $[Al(Ohfip)_4]^-$ [7, 14, 18]. A recent comprehensive review by Riedel et al. systematically compared various WCA-based RMMB electrolytes in terms of their electrochemical performance, stability, and synthetic feasibility [19]. Among them, $[B(Ohfip)_4]^-$ and $[Al(Ohfip)_4]^-$-based electrolytes are regarded as state-of-the-art systems owing to their well-balanced electrochemical and practical characteristics.

Concurrently, extensive efforts have been devoted to exploring solvents suitable for high-energy RMMBs. Ethereal solvents are generally considered the first choice because of their excellent compatibility with Mg electrodes. To further enhance the performance of ethereal electrolyte solutions, several strategies have been investigated, including structural modification of ether molecules to tune their physicochemical properties [20, 21], incorporation of additives and co-solvents in dual-solvent systems [22–28], and substitution of ethers with alternative solvent classes [29]. However, due to the limited compatibility of non-ethereal solvents with Mg electrodes [30], the co-solvent approach remains a feasible and promising route to meet diverse design requirements without compromising the inherent advantages of ethereal electrolytes. Among non-ethereal candidates, amines and their derivatives exhibit both high reductive stability and strong solvating ability. Although the beneficial effects of incorporating amine-based solvents into conventional ethereal RMMB electrolytes were first reported in the 1930s [31], this strategy has attracted renewed and growing attention in recent years [22, 25, 32–34]. Enhanced electrochemical performance, particularly at the Mg electrode interface, has been achieved by incorporating certain alkoxyalkylamines and alkyldiamines into conventional ethereal electrolytes. Comprehensive experimental and computational studies have revealed the critical influence of reactive nitrogen-bound hydrogen atoms within the amine molecular structure [35–37]. The formation of MgH_2-containing species, originating from parasitic reactions between primary or secondary amines and the Mg metal surface, promotes the development of compositionally graded inorganic–organic interphases accompanied by anion decomposition. These interphases effectively suppress further electrolyte decomposition while facilitating interfacial charge transfer, functioning analogously to conventional solid–electrolyte interphases (SEIs) [22, 25, 34]. Furthermore, Mg^{2+} coordination by amine molecules in solution markedly affects the rate-determining steps of Mg plating and stripping, including charge-transfer kinetics and the desolvation process [35].

Given the synergy demonstrated by recent advances in WCAs and amine co-solvents for RMMB electrolytes, the development of promising new electrolyte systems can be anticipated by combining these two groundbreaking concepts. In this work, we systematically examined the electrochemical characteristics of WCA-based ether–amine dual-solvent electrolytes and comprehensively investigated the influence of the paired anion species on their performance. Diglyme (G2) and 2-methoxyethylamine (MOEA) were adopted as benchmark solvents owing to their proven applicability in RMMB electrolytes and their favorable solubility for the studied salts (ESI; §3) [14, 18, 25, 34]. Two anions with distinctly different coordinating abilities—$[Al(Ohfip)_4]^-$ and $[TfO]^-$—representing weakly coordinating and strongly coordinating counterions, respectively, were selected to elucidate the role of anions in electrochemical and interfacial behaviors.

Unexpectedly, no beneficial synergistic effect was observed for the WCA–amine combination; rather, the system exhibited inferior electrochemical performance. Note that, due to its chemical nature as a base and a primary amine, MOEA typically contains higher amounts of hydrogen-bonded trace water that is difficult to remove or even quantify. In addition, this trace water may act as an acid toward the MOEA base and hence may form hydroxide ions and protonated MOEA in equilibrium. Both may possibly influence the electrolyte performance, as indicated by comprehensive interfacial analyses, combined with detailed insights into the coordination states of Mg^{2+} in solution. Our investigations revealed an MOEA-mediated trace-water-driven hydroxylation-based failure mechanism within the WCA–amine system, which is particularly critical for regulating the Mg electrode–electrolyte interface. Finally, the complex dilemma associated with developing next-generation electrolyte materials for RMMB applications is discussed with new facets.

2 | Results and Discussion

2.1 | Mg Plating/Stripping Performance and Morphological Evolution

Based on the preliminary compositional survey with respect to the salt solubility and primary electrochemical performance, a 1:1 (v/v) mixture of G2 and MOEA was employed as a benchmark solvent system. The chemistry behind the salt solubility and basic electrochemical properties is detailed in the electronic supporting information (ESI; §3 and Figures S1–S4). The electrochemical Mg plating/stripping performance of the electrolytes containing $Mg[Al(Ohfip)_4]_2$ and $Mg[TfO]_2$ salts were evaluated by systematic galvanostatic cycling and impedance measurements. The galvanostatic cycling results revealed a pronounced dependence of electrochemical performance on the nature of the anion. Unexpectedly, an electrolyte incorporating $[Al(Ohfip)_4]^-$ exhibited unstable Mg plating/stripping behavior, irrespective of the cell configuration, and these cells experienced short-circuiting at relatively early stages of cycling (Figure 1a). A similarly poor electrochemical performance was also observed for the electrolyte

21983844, 2026, 59, Downloaded from https://advanced.onlinelibrary.wiley.com/doi/10.1002/advs.76897 by Toshihiko Mandai - National Institute For , Wiley Online Library on [23/10/2026]. See the Terms and Conditions (https://onlinelibrary.wiley.com/terms-and-conditions) on Wiley Online Library for rules of use; OA articles are governed by the applicable Creative Commons License

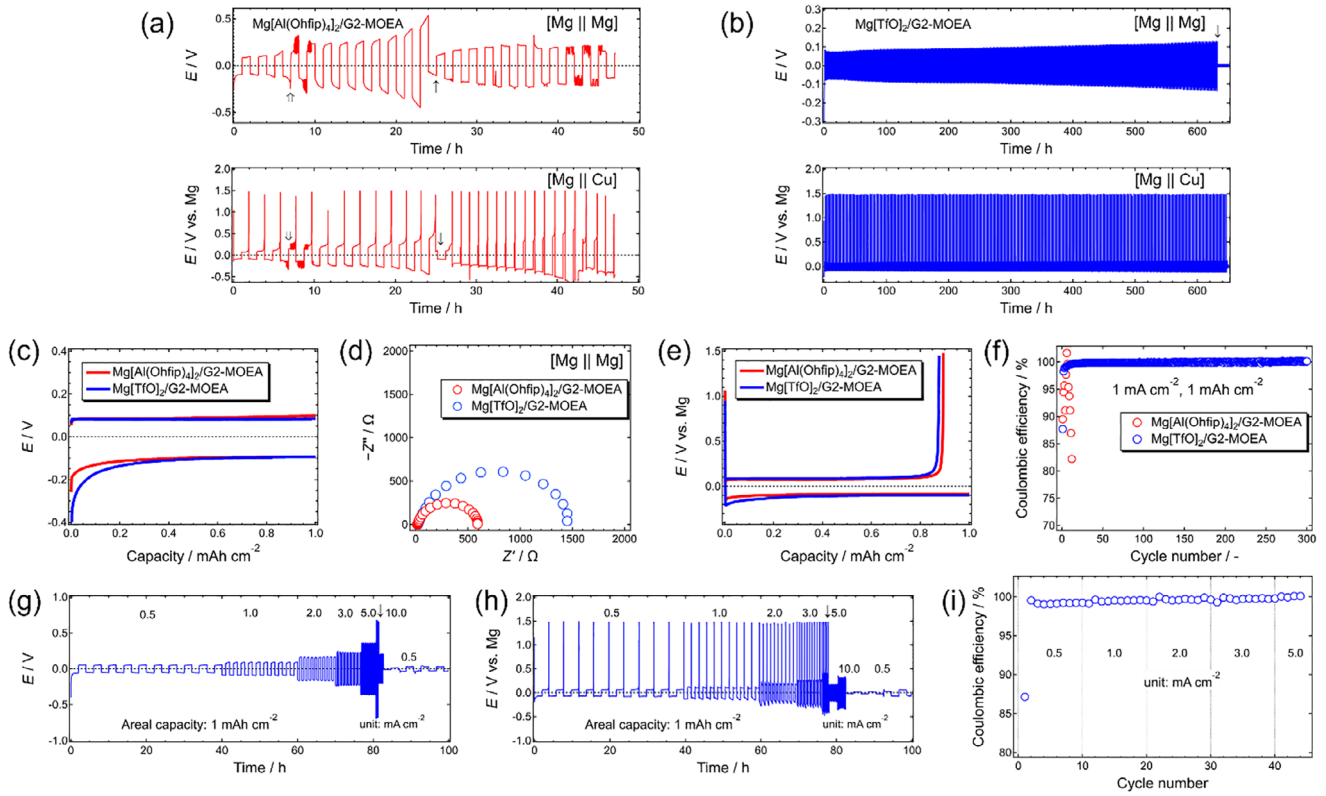


FIGURE 1 | (a, b) Galvanostatic Mg plating/stripping cycling profiles of symmetric [Mg || Mg] and asymmetric [Mg || Cu] cells using G2–MOEA-based electrolytes. Polarization curves of (c) symmetric and (e) asymmetric cells. (d) Electrochemical impedance spectra of symmetric cells before cycling. (f) Coulombic efficiencies. Rate capabilities of $Mg[TfO]_2$/G2-MOEA electrolytes with (g) symmetric and (h) asymmetric cells and (i) corresponding Coulombic efficiencies. Double arrows and single arrows in the cycling profiles indicate microshorts and definite shorts, respectively.

containing the structurally analogous $[B(Ohfip)_4]^-$ anion (Figure S5), indicating the limited compatibility of dual-solvent electrolyte systems with G2–MOEA and fluorinated alkoxyaluminate and alkoxyborate WCA-salts. In contrast, the coordinating-anion-based $Mg[TfO]_2$/G2-MOEA electrolyte displayed excellent Mg plating/stripping performance in both symmetric and asymmetric cell configurations. These cells exhibited highly stable cycling with minimal polarization for more than 600 h, even at a practical current density of 1 mA cm^{-2} (Figure 1b). The galvanostatic cycling-hold measurements further corroborate the greater static stability of the $Mg[TfO]_2$-based against the $Mg[Al(Ohfip)_4]_2$-based electrolyte (Figure S6).

A closer examination of the polarization behavior revealed that the electrolytes containing weakly coordinating $[Al(Ohfip)_4]^-$ and strongly coordinating $[TfO]^-$ anions exhibited similar characteristics, regardless of the cell configuration. The overpotential for Mg plating and stripping stabilized at approximately 80 mV after the initial nucleation stage. The difference in the depth of the nucleation overpotential between the $Mg[Al(Ohfip)_4]_2$- and $Mg[TfO]_2$-based electrolytes—more pronounced in the symmetric cell configuration (Figure 1c)—is most likely attributable to their distinctly different interfacial impedances, as shown in Figure 1d. The smaller interfacial charge-transfer resistance observed for the $Mg[Al(Ohfip)_4]_2$-based electrolyte corresponds to the shallowest nucleation overpotential. The Coulombic efficiency for Mg plating/stripping during the first cycle was also nearly identical between these two electrolytes (around 90%); however, their long-term cycling stability differed significantly. The Coulombic efficiency of the $Mg[Al(Ohfip)_4]_2$/G2-MOEA electrolyte fluctuated throughout the first 13 cycles (Figure 1f), and micro-short-circuiting events, possibly arising from inhomogeneous Mg plating/stripping reactions (vide infra), were observed. In contrast, the efficiency of the $Mg[TfO]_2$/G2-MOEA electrolyte stabilized rapidly after the initial formation and activation processes, approaching 99.9% in subsequent cycles. This electrolyte also demonstrated outstanding Mg plating/stripping performance even at higher current densities, up to 5 mA cm^{-2}, regardless of the cell configuration examined (Figure 1g,i).

The morphological characteristics of the deposits reflect the differences in electrochemical performance among the electrolytes. As shown in Figure S7, crystalline granular deposits with an average size of less than 10 μm were formed on the substrates regardless of the electrolyte type; however, their surface morphology differed significantly. The magnified scanning electron microscopy (SEM) images revealed that, in the $Mg[Al(Ohfip)_4]_2$-based electrolyte, highly crystalline angular primary particles coalesced (Figure S7b), whereas in the $Mg[TfO]_2$-based, smaller primary crystals fused together to form rounded secondary particles (Figure S7d). Subsequent powder X-ray diffraction (pXRD) analysis confirmed successful plating of hcp-Mg with high crystallinity and almost identical crystal orientation on the substrates in both electrolytes (Figure S7e). Despite exhibiting similar electrochemical Mg plating behavior, the weakly coordinating $Mg[Al(Ohfip)_4]_2$ and the strongly coordinating $Mg[TfO]_2$

21983844, 2026, 59, Downloaded from https://advanced.onlinelibrary.wiley.com/doi/10.1002/advs.76897 by Toshihiko Mandai - National Institute For , Wiley Online Library on [23/10/2026]. See the Terms and Conditions (https://onlinelibrary.wiley.com/terms-and-conditions) on Wiley Online Library for rules of use; OA articles are governed by the applicable Creative Commons License

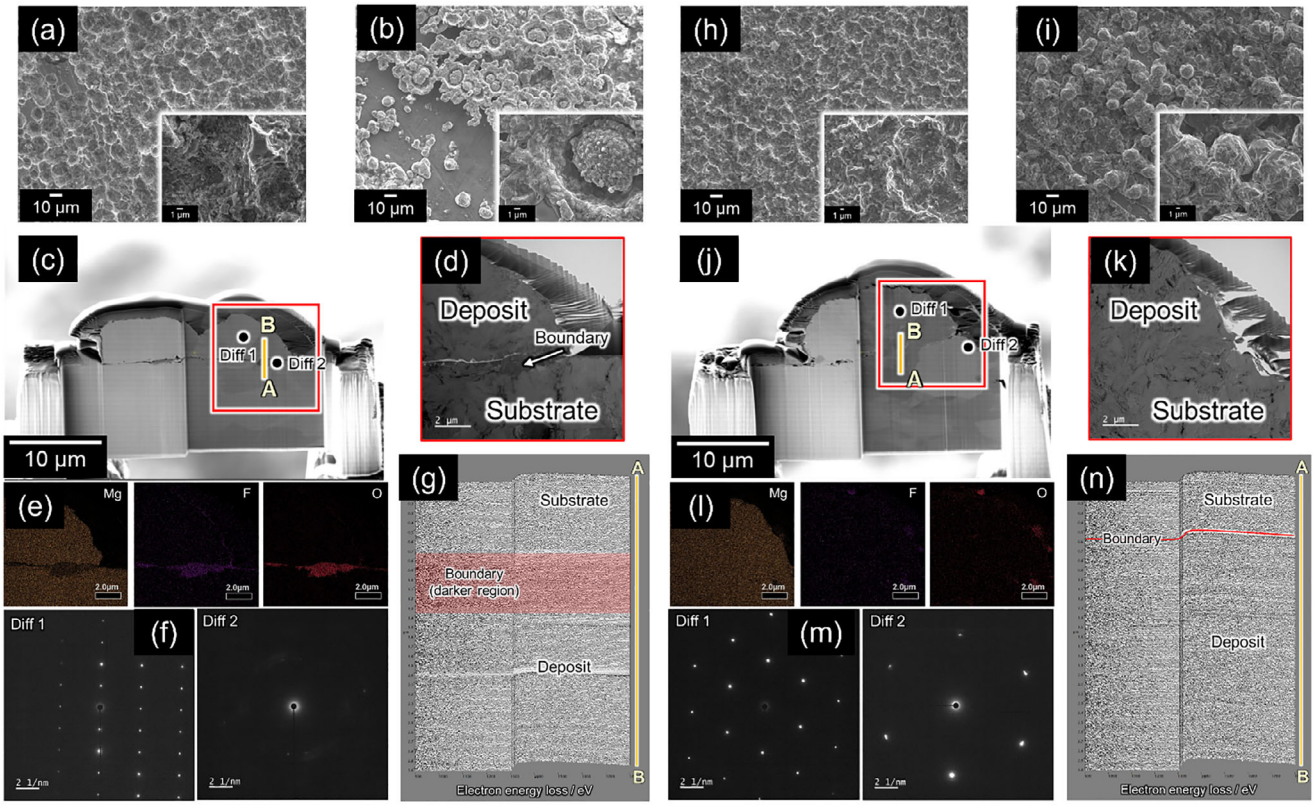


FIGURE 2 | SEM and STEM analyses of Mg metals after electrochemical stripping–plating reactions conducted in (a–g) $Mg[Al(Ohfip)_4]_2$/G2-MOEA and (h–n) $Mg[TfO]_2$/G2-MOEA electrolytes. Surface SEM images of Mg metals after (a, h) a single stripping process and (b, i) one stripping–plating cycle at a current density of 1 mA cm^{-2} and a geometrically fixed areal capacity of 1 mAh cm^{-2}. Cross-sectional (c, j) SEM images and the corresponding (d, k) STEM images, (e, l) EDX mappings, (f, m) position-resolved electron diffraction patterns, and (g, n) EELS spectra of the deposits and substrates are shown. The positions of STEM observations, diffraction measurements, and EELS analyses are indicated in (c) and (j).

electrolytes showed a pronounced difference in their long-term plating/stripping performance (Figure 1a,b). These observations strongly suggest that interfacial stability largely depends on the coordinating characteristics of the anions in the electrolyte solution and potentially also the capacities of the system to interact with the trace water present, e.g., by deprotonation and hydroxide formation (vide infra.).

Repeated stripping and plating cycles inevitably induce successive morphological changes in the metal electrodes. The characteristic plating behavior of Mg on substrates containing pits is widely recognized as a critical issue in the field of RMMBs, because such localized plating results in a markedly rough surface [13, 38–41]. This roughness, in turn, severely limits the active surface utilization and increases the risk of short-circuiting through the intrusion of metallic Mg into porous separators. The surface morphology of Mg after a single stripping–plating cycle in the $Mg[Al(Ohfip)_4]_2$-based electrolyte clearly exhibited this characteristic feature, as shown in Figure 2a,b. The deposits preferentially accumulated around the pits formed during the previous stripping process, while granular deposits were also observed both inside the pits and on the unreacted surface areas. As Mg tends to deposit preferentially on less resistive areas [42], this observation suggests spatially inhomogeneous passivation. The surface image obtained after a single stripping–plating cycle also indicated partial detachment of the deposits from the substrate (Figure 2b). A similar low-adhesive behavior has also been reported for Mg deposited after a single plating process—without a preceding stripping step—in the MOEA-free ethereal $Mg[Al(Ohfip)_4]_2$/G2 electrolyte [40]. The adhesion of the deposits to the substrate is particularly important for long-term cycling stability, as weakly adherent deposits can easily lose physical contact with the substrate, forming electrically isolated "dead" Mg, which in turn leads to poor Coulombic efficiency and an increased risk of short-circuiting upon percolation. Fractured "dead" Mg was directly observed in the [Mg || Mg] symmetric cells with the $Mg[Al(Ohfip)_4]_2$/G2-MOEA electrolyte during repeated plating and stripping cycles by in situ electrochemical confocal microscopy (vide infra). The cross-sectional view of the deposits on the substrate provided additional insights into the stripping–plating behavior. Figure 2c shows the cross-sectional SEM image of the Mg electrode after a single stripping–plating cycle, obtained using a focused ion beam technique. Semicircular, granular Mg particles were deposited on the underlying Mg substrate. The corresponding high-resolution scanning transmission electron microscopy (STEM) image, together with position-resolved electron diffraction, energy-dispersive X-ray spectroscopy (EDX), and electron energy loss spectroscopy (EELS), clearly revealed the formation of an oxygen- and fluorine-containing amorphous phase at the interface between the deposits and the substrate (Figure 2d–g).

In the case of the $Mg[TfO]_2$-based electrolyte, granular Mg deposits were observed uniformly across the substrate after a

21983844, 2026, 59, Downloaded from https://advanced.onlinelibrary.wiley.com/doi/10.1002/advs.76897 by Toshihiko Mandai - National Institute For , Wiley Online Library on [23/10/2026]. See the Terms and Conditions (https://onlinelibrary.wiley.com/terms-and-conditions) on Wiley Online Library for rules of use; OA articles are governed by the applicable Creative Commons License

single stripping–plating cycle (Figure 2i). Such distinct deposition behavior suggests the distinct interfacial chemistries between the $Mg[Al(Ohfip)_4]_2$- and $Mg[TfO]_2$-based electrolytes. The detailed cross-sectional STEM image, combined with subsequent comprehensive analyses, demonstrated favorable Mg plating behavior in the $Mg[TfO]_2$-based electrolyte. Only a very limited amorphous phase was detected at the interface between the deposits and the substrate, as confirmed by EDX, position-resolved electron diffraction, and EELS analyses (Figure 2l–n). These observations strongly suggest the formation of a stable interfacial layer in the $Mg[TfO]_2$-based electrolyte.

Visual observation is a powerful learning tool, especially in the field of battery research. Directly monitoring the dynamic plating and stripping processes provides crucial insights into interfacial behavior and morphological evolution across different electrolytes. To visualize the Mg plating/stripping behavior under operating conditions, a specially designed electrochemical cell was fabricated in a symmetric [Mg || Mg] configuration, incorporating a conventional glass fiber separator. Galvanostatic cycling measurements were then performed under a confocal microscope. As shown in Videos 1 and 2 deposited with the supporting information, the dynamic behavior varied significantly depending on the electrolyte used. In the case of the $Mg[Al(Ohfip)_4]_2$-based electrolyte (Video 1), the electrode surfaces were already damaged by the electrolyte prior to electrochemical measurements, and fractured Mg particles had penetrated into the porous separator. The exposed electrode surface gradually responded to the applied current, and localized plating and subsequent stripping of Mg metal were observed at the facing Mg electrodes, accompanied by minimal gas evolution. The snapshots captured at specific reaction intervals further supported these dynamic observations (Figure S8). The cell experienced an undesired short circuit during the third plating/stripping cycle, as evidenced by irregular voltage fluctuations, although this event was unfortunately not visible within the observed field. This observation is in good agreement with the unstable electrochemical performance shown in Figure 1a. The percolation of isolated Mg particles through localized, uneven plating/stripping likely accelerated the short-circuit event. In contrast, surface reactions accompanied by significant gas evolution (bubbling) initiated immediately after the current was applied in the cell employing the $Mg[TfO]_2$-based electrolyte (Video 2). These observations suggest that surface reactions are likely accelerated by freshly exposed, thus highly active Mg^0 in this electrolyte. Spatially homogeneous plating and stripping reactions were also evident from the operando observations. Notably, plating and stripping in the $Mg[TfO]_2$-based electrolyte were always accompanied by continuous bubbling. This finding implies a strong correlation between gas evolution and the uniformity of Mg plating and stripping, because the cells employing the $Mg[Al(Ohfip)_4]_2$-based electrolytes with and without MOEA—where little or no bubbling was observed during repeated plating/stripping cycles—exhibited uneven utilization of the Mg electrodes (Video 1 and Video S1). The critical role of reactive amine protons in alkylamines in influencing Mg plating and stripping has been experimentally supported in previous studies [22, 23, 36]. The observed results indicate that either the amine protons of MOEA or the potentially present Mg-coordinated trace water exhibit greater reactivity in the $Mg[TfO]_2$-based electrolyte, and this enhanced reactivity promotes the formation of a functional interfacial layer. In contrast, such reactivity appears to be suppressed in the $Mg[Al(Ohfip)_4]_2$-based electrolyte.

It has been reported that replacing the moderately coordinating $[TFSA]^-$ into strongly coordinating $[TfO]^-$ anions in amine-based electrolytes can weaken the H_2 evolution through -NH_2 reduction, and this effectively enhances the stability of the Mg-electrolyte interface [25]. The recent combined theoretical and spectroscopic studies on the Mg salt-ether-amine systems, however, suggested the dominant role of free or loosely-bound amine solvents for inducing H_2 gas evolution and associated MgH_2 formation to stabilize the interface [34, 37]. A competition in coordination to Mg^{2+} among amine, ether, and counterions seems important to stabilize the interface by amine decomposition, as the single amine solvent systems, where the dominant species in electrolyte solutions should be Mg-amine solvates, exhibited substantially poor performance compared to the corresponding dual amine-ether solvent systems. The present study also points out that the combined presence of water and amine with the strongly coordinating $[TfO]^-$ anions would drive gas evolution (vide infra). As the present and preceding works draw somewhat different conclusions with respect to the mechanisms of H_2 gas evolution and stabilization of the Mg-electrolyte interface, and more importantly, water contents of respective electrolyte solutions are unclear, further detailed compositional and mechanistic studies with an aid of computational approaches combined with advanced operando characterization techniques are necessary to fully understand the interfacial chemistry in Mg-amine systems.

The importance of reactive amine protons or the trace-water-based reactivity in the presence of amines—rather than merely the interfacial composition—toward electrochemical Mg plating and stripping was also supported experimentally. Indeed, no significant improvement in plating/stripping performance was observed for the MOEA-free $Mg[Al(Ohfip)_4]_2$/G2 electrolyte, even when Mg electrodes previously cycled in the $Mg[TfO]_2$-based electrolyte were used for the subsequent measurements (Figure S9). As the amine-trace water proton-driven surface reaction consumes active amine molecules in electrolyte solutions [43], the cycle life of the cells is dominated by the amount of electrolyte. To achieve the sufficiently stable cycling of Mg electrodes, a statically stable interface is necessary to be developed.

2.2 | Solvation State and Interfacial Chemistry

The distinct solvation environments of G2 and MOEA in $Mg[Al(Ohfip)_4]_2$/G2-MOEA and $Mg[TfO]_2$/G2-MOEA electrolytes were investigated by ^1H NMR spectroscopy (Figure S10). The amine proton (—NH_2) resonance at 1.2 ppm showed only slight upfield shift upon mixing with G2, indicating weak G2–MOEA interactions. Downfield shifts of the —NH_2, methoxide, and methylene groups confirm MOEA–Mg^{2+} interactions that differ by salt. In the $Mg[Al(Ohfip)_4]_2$-based system, ether oxygen (methoxide) atoms of MOEA bind stronger to Mg^{2+} (—NH_2 downfield shift: 0.6 ppm), while in $Mg[TfO]_2$, the larger 1.3 ppm —NH_2 shift indicates —N(H)-*H*···X H-bonding presumably involving $[TfO]^-$ oxygen atoms, confirming MOEA participation in Mg^{2+} solvation via anion interaction, consistent with earlier MD simulations [34]. Single-solvent MOEA spectra (Figure S11) show analogous trends. The small G2 chemical shift

21983844, 2026, 59, Downloaded from https://advanced.onlinelibrary.wiley.com/doi/10.1002/advs.76897 by Toshihiko Mandai - National Institute For , Wiley Online Library on [23/10/2026]. See the Terms and Conditions (https://onlinelibrary.wiley.com/terms-and-conditions) on Wiley Online Library for rules of use; OA articles are governed by the applicable Creative Commons License

changes in the $Mg[Al(Ohfip)_4]_2$-based electrolyte indicate minor G2 participation in Mg^{2+} complexation within fast exchange equilibria, consistent with the absence of non-coalescent solvent signals on the time scale of NMR measurements.

In the WCA-based electrolytes, Mg^{2+} is preferentially solvated by solvent molecules due to the low associativity of WCAs. Small (C—)H chemical shift changes for both G2 and MOEA confirm dual-solvent participation in Mg^{2+} solvation. Without strong H-bonding to $[Al(Ohfip)_4]^-$, the 0.6 ppm —NH_2 low-field shift identifies MOEA as the preferred Mg^{2+} ligand via NH_2 coordination, but still being in rapid equilibrium with G2. By contrast, strong Mg^{2+}–$[TfO]^-$ association (confirmed by Walden plots from conductivity and viscosity measurements, Figure S12) shields Mg^{2+} and likely excludes G2 coordination in the $Mg[TfO]_2$-based electrolyte, consistent with unchanged ^1H NMR signals of G2. As a known H-bond acceptor (HBA) [44], $[TfO]^-$ attracts the positively polarized amine protons of Mg^{2+}-coordinated MOEA through H-bonding, as further investigated by Raman spectroscopy.

Raman analysis of the $Mg[TfO]_2$/G2-MOEA electrolyte (Figure S13) focused on the CF_3 symmetric bending mode $\delta_s(CF_3)$, sensitive to ion-pair formation [45–47]. Voigt deconvolution yielded two modes at 767 and 761 cm^{-1}, with no signal in the 757–740 cm^{-1} range, confirming the absence of any "free", non-coordinated $[TfO]^-$ (reference: 752 cm^{-1} for $[N(Bu)_4]^+$ salt [48]). The blueshifted 767 cm^{-1} mode corresponds to strongly associated $[TfO]^-$, and the 761 cm^{-1} mode—consistent with hydrogen-bonded $[TfO]^-$ near 762 cm^{-1} in dialkylimidazolium systems [47]—supports HBA action of $[TfO]^-$ and corroborates (H)N-H···O-S H-bonding between $[TfO]^-$ and the NH_2 group of MOEA in the $[Mg(MOEA)_n]^{2+}$ complex.

HF-DFT calculations at the RI-B3LYP(D3BJ)/def2-TZVPP level with COSMO implicit solvation (ε_r = 7.23 for G2) [49] and extra explicit solvent molecules were performed to support the spectroscopic findings. Thermodynamic values are reported in solution ($\Delta_r G°$ at 298 K; all deposited in §2.1 ESI). For the $Mg[Al(Ohfip)_4]_2$/G2-MOEA system (evaluated to always exhibit coordination number 6), the global minimum is $[Mg(MOEA)_3]^{2+}$; $[Mg(G2)_2]^{2+}$ lies +11 kJ mol^{-1} higher. With $\Delta_r G°(\text{solution}) = -RT$ ln K, the equilibrium constant K is $10^{-1.93}$, implying only 1 out of 85 Mg^{2+} ions takes up G2 at equilibrium. For the $Mg[TfO]_2$/G2-MOEA system, the solvation structures of which were previously elucidated [25, 34], our calculations agree with prior work: the tight ion pair $[Mg(MOEA)_2(TfO)_2]$ is the dominant species, and all G2-containing structures are much higher in energy (Table S2). Conversion to the free $[Mg(MOEA)_3]^{2+}$ ion (which dominates in the $Mg[Al(Ohfip)_4]_2$/G2-MOEA electrolyte) costs ca. 170 kJ mol^{-1} in Gibbs energy, confirming that $[TfO]^-$ ions persist in the Mg^{2+} environment, primarily as the tight ion pair $[Mg(MOEA)_2(TfO)_2]$ and, as a very minor component, H-bonded $[Mg(MOEA)_3(TfO)_2]$, that is ca. 40 kJ mol^{-1} higher in energy.

To elucidate the impact of the solvation state on the interfacial characteristics of the $Mg[Al(Ohfip)_4]_2$ and $Mg[TfO]_2$-based electrolytes, comparative studies were conducted. Figure 3 presents SEM images of Mg metal soaked in these two electrolytes for 48 h. Evidently, the Mg surface was damaged due to reactions with the alkoxyalkylamine-integrated electrolyte solutions, whereas no significant change in surface morphology was observed for Mg metal soaked in the MOEA-free $Mg[Al(Ohfip)_4]_2$/G2 electrolyte (Figure 3 and Figure S14). Subsequent X-ray photoelectron spectroscopy (XPS) analysis of the soaked Mg metals, however, revealed distinct reaction mechanisms between the $Mg[Al(Ohfip)_4]_2$- and $Mg[TfO]_2$-based electrolytes. For the $Mg[Al(Ohfip)_4]_2$-based electrolyte, the metallic Mg surface is well exposed, and the residual surface composition was dominated by oxygen-based compounds such as MgO and $Mg(OH)_2$ [50]. The larger relative content of Mg(0) against Mg-oxygen compounds and the negligible contribution of nitrogen- and fluorine-containing species to the surface composition strongly suggests that the native oxygen-based surface layer was removed through an etching effect, while the MOEA solvent and the $[Al(Ohfip)_4]^-$ anion do not likely decompose during this etching process (vide infra for its mechanism). The etching behavior of the $Mg[Al(Ohfip)_4]_2$-based electrolyte is further supported by the exceptionally small interfacial resistance (Figure 1d). In contrast, for the $Mg[TfO]_2$-based system, various elements including fluorine, nitrogen, and oxygen significantly contributed to the formation of a more complex surface layer. Notably, this layer consisted of both organic (C-NH_2 and CF_3) and inorganic (MgF_2, $Mg(NO_x)_2$, and $Mg(OH)_2$) species [13, 50]. These observations clearly indicate that both the MOEA solvent and the $[TfO]^-$ anion participated in the surface reactions. The formation of a hybrid organic–inorganic interface through preferential decomposition of the MOEA-coordinated Mg^{2+} complex, accompanied by $[TfO]^-$ decomposition, has also been reported in previous studies [25, 34]. The resulting hybrid interface, enriched with relatively insulating components, is responsible for the substantially larger interfacial resistance observed for Mg metal in the $Mg[TfO]_2$/G2-MOEA electrolyte (Figure 1d).

In addition to these conventional interfacial components, metal hydrides originating from parasitic interfacial reactions have recently been identified as functional agents in Mg plating and stripping processes [22, 23, 36, 37]. Because hydrogen ions are difficult to detect by XPS, time-of-flight secondary ion mass spectrometry (TOF-SIMS) analysis was conducted on the same Mg metal samples used for the XPS measurements. Figure 3e,f presents the depth profiles of TOF-SIMS spectra obtained in the positive and negative ion modes, respectively. The positive-mode profiles indicate a minimal contribution of metal hydrides to the surface layer composition. Hydride species were detected even in pristine Mg metal, and their relative intensities remained almost unchanged across the Mg samples soaked in different electrolytes. Taking a closer look at the SIMS profiles, particularly at the outermost surface (sputter time = 0 s), the mass signals assignable to MgH^+ appear slightly higher for the sample soaked in $Mg[Al(Ohfip)_4]_2$/G2-MOEA than for those soaked in $Mg[TfO]_2$/G2-MOEA. However, such a minor difference is insufficient to account for the substantially larger disparity in the interfacial characteristics of these two electrolytes. In contrast to the positive-ion mode, the negative-ion mode profiles clearly revealed compositionally distinct interlayer formations on the Mg surfaces soaked in the $Mg[Al(Ohfip)_4]_2$- and $Mg[TfO]_2$-based electrolytes. The surface of the Mg metal soaked in the $Mg[Al(Ohfip)_4]_2$-based electrolyte was enriched with oxygen-containing compounds, whereas significant contributions from fluorine- and nitrogen-containing species were observed in the sample derived from the $Mg[TfO]_2$-based electrolyte. Notably,

21983844, 2026, 59, Downloaded from https://advanced.onlinelibrary.wiley.com/doi/10.1002/advs.76897 by Toshihiko Mandai - National Institute For , Wiley Online Library on [23/10/2026]. See the Terms and Conditions (https://onlinelibrary.wiley.com/terms-and-conditions) on Wiley Online Library for rules of use; OA articles are governed by the applicable Creative Commons License

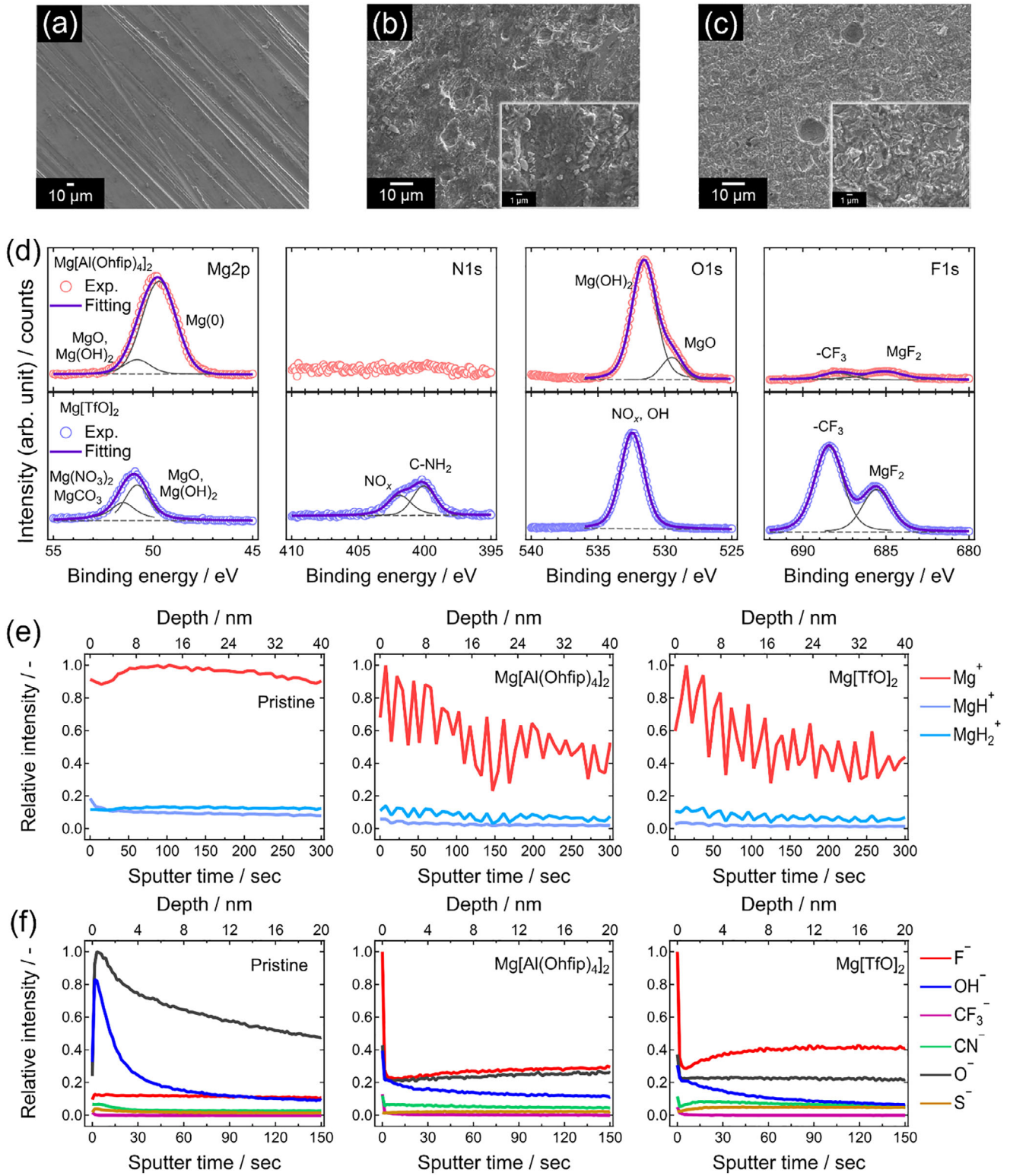


FIGURE 3 | Surface SEM images of (a) pristine Mg and Mg metals soaked in (b) $Mg[Al(Ohfip)_4]_2$/G2-MOEA and (c) $Mg[TfO]_2$/G2-MOEA. (d) Mg 2p, N 1s, O 1s, and F 1s (left to right) XPS spectra of Mg electrodes soaked in (upper) $Mg[Al(Ohfip)_4]_2$/G2-MOEA and (lower) $Mg[TfO]_2$/G2-MOEA. Depth-profiled SIMS spectra of pristine Mg and Mg metals soaked in the two electrolytes were acquired in (e) positive and (f) negative ion modes. The samples used for these characterizations were prepared by soaking mechanically polished Mg metals in the respective electrolytes for 48 h at 30°C.

21983844, 2026, 59, Downloaded from https://advanced.onlinelibrary.wiley.com/doi/10.1002/advs.76897 by Toshihiko Mandai - National Institute For , Wiley Online Library on [23/10/2026]. See the Terms and Conditions (https://onlinelibrary.wiley.com/terms-and-conditions) on Wiley Online Library for rules of use; OA articles are governed by the applicable Creative Commons License

substantially larger contributions of CN^- and S^- were discernible for the $Mg[TfO]_2$/G2-MOEA electrolyte (Figure 3f). These findings are in good agreement with the results of the XPS analysis (Figure 3d). Considering the electrochemical and analytical results together, it can be concluded that the nitrogen- and fluorine-containing interfacial components derived from MOEA and $[TfO]^-$ play a crucial role in stabilizing the Mg/electrolyte interface by suppressing further parasitic reactions during Mg plating and stripping cycles.

The distinct compositions of the Mg–electrolyte interfaces in $Mg[Al(Ohfip)_4]_2$/G2-MOEA and $Mg[TfO]_2$/G2-MOEA systems can thus be rationalized in terms of their respective solution states. It is well recognized, particularly in RMMB research, that species coordinated to Mg^{2+} become highly susceptible to reduction because of the strong electric field exerted by Mg^{2+} and the resulting large shift in the electron affinity of the coordinating species [20, 51, 52]. In $Mg[Al(Ohfip)_4]_2$/G2-MOEA, the theoretical calculations suggest $[Mg(MOEA)_3]^{2+}$ to be the dominant species. Upon electronation, the Löwdin population analysis of the vertical radical cation emphasizes that the $[Mg(MOEA)_3]^{\cdot+}$ ion has a coefficient directly at the Mg atom (see §2.2 ESI). As the higher spin density on Mg and the NH_2 groups stabilize the electron density through effective spin-delocalization – similar to the high stability of even free solvated electrons in solutions of alkaline or alkaline earth metals in ethylene diamine $H_2N\text{-}CH_2CH_2\text{-}NH_2$ [53, 54], a $[Mg(MOEA)_3]^{\cdot+}$ radical cation yields Mg-metal presumably directly plated on the interface with almost no decomposition products upon reduction at the Mg interface. This agrees with the absence of any nitrogen signature in the XPS analysis (Figure 3d). Because $[Al(Ohfip)_4]^-$ remains outside the primary solvation sheath of Mg^{2+}, it retains its intrinsic reductive stability in solution. Yet, if the highly polarized coordinated G2 molecules in the $[Mg(G2)_2]^{2+}$ ion available in equilibrium accept electrons from the reductive Mg metal surface at the interface, the electrons taken up by the system are much higher in energy, thus more reactive and likely induce ligand-degradation. Consequently, the surface of Mg metal in contact with $Mg[Al(Ohfip)_4]_2$/G2-MOEA slowly and over time becomes enriched with G2-derived oxygen-containing compounds, as evidenced by the XPS spectra (Figure 3d). In contrast, $[TfO]^-$ participates strongly in the solvation of Mg^{2+} and the $\text{-}NH_2$ group of MOEA is further bound to $[TfO]^-$ via H-bonding in the $Mg[TfO]_2$-based electrolyte. Such a multi-compositional solvation structure promotes the decomposition of both $[TfO]^-$ and MOEA at the Mg metal surface, leading to the formation of the observed fluorine- and nitrogen-rich functional interface.

2.3 | MOEA-Mediated Partial Hydroxylation of $[Al(Ohfip)_4]^-$ and Understanding of Dynamic Failure Mechanism in $Mg[Al(Ohfip)_4]_2$/G2-MOEA

During the NMR investigations, a peculiar water-induced hydroxylation process of the $[Al(Ohfip)_4]^-$ ion was detected. Note that, despite adopting an intensive dehydration protocol to MOEA for this study – i.e., by distillation over CaH_2 and storage with activated molecular sieves for several days – the water content in our MOEA solvent batches was indirectly determined to spread between several hundred to several thousand ppm based on the NMR analysis, where all products formed were assumed to originate from the reaction of $[Al(Ohfip)_4]^-$ with water remnants in MOEA. To further support this point, we have investigated the water content in the MOEA batch used by a titration protocol in the presence of benzoic acid, that is reported bind all the basic MOEA amine, and only leaves the less basic water unaffected and to be determined [55]. This protocol gave a water content of 156 ppm in MOEA. As the MOEA was mixed with G2 in 1:1 volume ratio in our electrolyte formulations, the water content in $Mg[Al(Ohfip)_4]_2$/G2-MOEA is assumed to be less than 150 ppm. However, these values are not very trustworthy in our opinion, as they depend much on the titration criteria applied (details of the titration protocol and criteria are given in the ESI). By contrast, water contamination of the $Mg[Al(Ohfip)_4]_2$/G2 electrolyte does not significantly affect Mg plating/stripping performance and the $[Al(Ohfip)_4]^-$ anion tolerates even 1000 ppm water content with no visible byproduct as shown by NMR [18]. Since this work showed the somewhat moist $Mg[Al(Ohfip)_4]_2$/G2-MOEA electrolyte to support Mg plating and stripping (Figures 1 and 2), its water content seems to lie still below the direct hydrolysis threshold of the $[Al(Ohfip)_4]^-$ anion [18, 27]. Therefore, MOEA apparently plays a crucial role in enabling the hydroxylation of $[Al(Ohfip)_4]^-$.

With this background, the stability of the $[Al(Ohfip)_4]^-$ ion in the presence of water and amine was investigated in solution. As shown in Figure 4a, $Mg[Al(Ohfip)_4]_2$ in G2 exhibits a characteristic septet ^1H resonance at 4.5 ppm, which is assignable to the α-proton of the $O\text{-}C(H)(CF_3)_2$-group. However, an additional downfield resonance appears in the G2–MOEA solution that is assigned to a reaction product with $[Al(Ohfip)_4]^-$. The corresponding ^{19}F NMR spectrum confirms the formation of another Ohfip-compound and the sharp ^{27}Al resonance arising from the tetracoordinated environment (Al_{CN4}) in $Mg[Al(Ohfip)_4]_2$/G2 is now flanked by an additional broader signal at approximately 30 ppm in the presence of MOEA/trace water. The shift position at 30 ppm agrees with a penta-coordinated structure [56]. For example, the trigonal bipyramidal aluminate anion $[F_2Al(Ohfip)_3]^{2-}$, has a distinct ^{27}Al NMR signal at 33.7 ppm [57] (replace fluoride by isosteric hydroxide). Also a dimeric $[(hfipO)_3Al\text{-}(\mu\text{-}F)_2\text{-}Al(Ohfip)_3]^{2-}$ is known [57], unfortunately without NMR shift. If one again replaces F for OH, this could suggest dimerization of an initial tetracoordinate $[Al(Ohfip)_3(OH)]^-$ (cf. the known [58], bulkier $[Al(OC(CF_3)_3)_3(OH)]^-$) to give the pentacoordinate (Al_{CN5}) $[(hfipO)_3Al\text{-}(\mu\text{-}OH)_2\text{-}Al(Ohfip)_3]^{2-}$ dianion. From diffusion-ordered NMR spectroscopy measurements (data not shown), the formation of a large complex anion, diffusing slower than monomeric $[Al(Ohfip)_4]^-$, agrees with the assignment of dimeric $[(hfipO)_3Al\text{-}(\mu\text{-}OH)_2\text{-}Al(Ohfip)_3]^{2-}$, (as its Mg^{2+} complex?), as the pentacoordinate aluminate in solution. Also partial hydrolysis of the parent $Mg[Al(Ohfip)_4]_2$•3G1 adducts is known to yield a binuclear aluminate anion [59]. In addition, solvent coordination may induce formation of penta-coordinated Al species [60].

The relative intensities of the reaction products – the Ohfip-compound and the penta-coordinate Al species – are higher in the single MOEA-solvent system than in the mixed G2–MOEA solvent system (Figure 4), confirming that the reaction with $[Al(Ohfip)_4]^-$ is significantly promoted by MOEA. Nevertheless, quantitative analysis of the relevant signal areas indicates that only about 20% of $[Al(Ohfip)_4]^-$ undergoes reaction. Even an

21983844, 2026, 59, Downloaded from https://advanced.onlinelibrary.wiley.com/doi/10.1002/advs.76897 by Toshihiko Mandai - National Institute For , Wiley Online Library on [23/10/2026]. See the Terms and Conditions (https://onlinelibrary.wiley.com/terms-and-conditions) on Wiley Online Library for rules of use; OA articles are governed by the applicable Creative Commons License

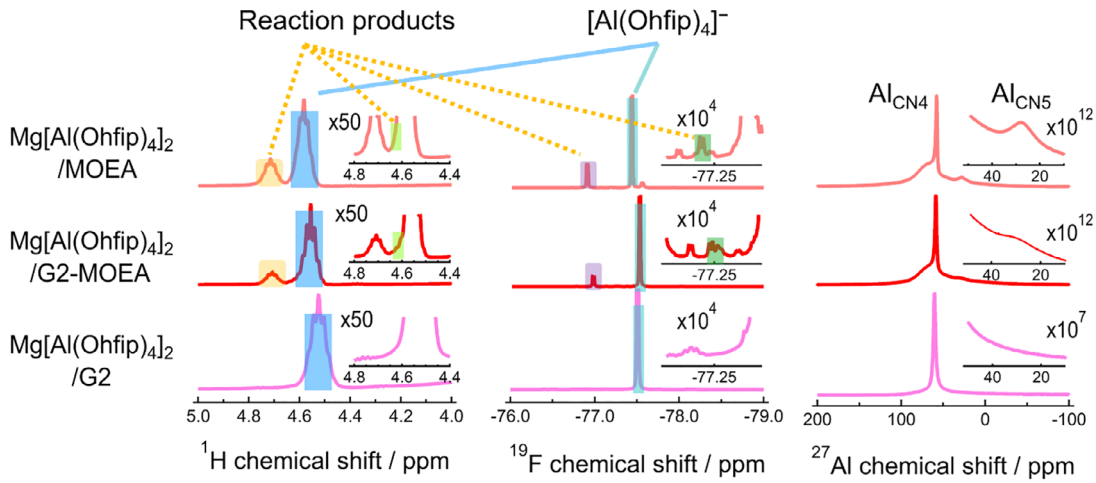


FIGURE 4 | ^{1}H, ^{19}F, and ^{27}Al NMR (25°C; either 400.17, 376.54, and 104.27 MHz or 300.18, 282.45, and 78.22 MHz, respectively) spectra of $Mg[Al(Ohfip)_4]_2$-based electrolytes. Selected spectral regions corresponding to $[Al(Ohfip)_4]^-$ are highlighted. Al_{CN4} and Al_{CN5} denote Al species with a coordination number of 4 and 5, respectively. The intensive broad resonance between 0 and 100 ppm in the ^{27}Al-NMR spectrum is a background signal from the probehead, whereas the small broad shoulder at 30 ppm is a signal from the sample.

intentionally added far excess of water (ca. 0.5 mol dm^{-3}!), which would have been enough to react with all $[Al(Ohfip)_4]^-$ in the electrolyte, shows that only about 20% of $[Al(Ohfip)_4]^-$ undergoes reaction (Figure S15) in the $Mg[Al(Ohfip)_4]_2$/G2-MOEA solutions. Moreover, the reaction reaches completion immediately after sample preparation, as aging has no discernible effect on the relative composition of $[Al(Ohfip)_4]^-$ and its reaction products (cf. identical NMR spectra of as-prepared and aged samples; Figure S16). These observations suggest a peculiar reaction mechanism driven by the water-contaminated MOEA and $[Al(Ohfip)_4]^-$.

Further Fourier transform attenuated total reflection infrared (FT-ATR-IR) spectroscopy measurements of the electrolyte shown in Figure S17 verify a collective large redshift of the N-H vibrational modes in the $Mg[Al(Ohfip)_4]_2$/G2-MOEA system. This strongly suggests protonation of MOEA resulting in strong H-bonding visible by IR. Hence, also protonated MOEA ($[H\text{-}MOEA]^+$) appears to be relevant as part of this reaction.

To identify the underlying cause of the undesired water-induced reaction of $[Al(Ohfip)_4]^-$, the Gibbs free reaction energies ($\Delta_r G°$) of possible reaction products were DFT calculated in G2 solution as described above [49]. Since MOEA is chemically a base (cf. pK_a of its protonated form in water: 9.40 [61]), it may react in an acid-base equilibrium with water to yield hydroxide (reaction (1), with hydration of the cation being considered). The nucleophilic hydroxide ion formed in (1) could then attack the electrophilic Al-atom of the $[Al(Ohfip)_4]^-$ anion (2):

$$\mathrm{MOEA_{(solv.)} + 2H_2O_{(solv.)} \rightleftarrows [H_2O\cdots H - MOEA]^+_{(solv.)} + HO^-_{(solv.)} \quad \Delta_r G°(1) = +6\ kJ\ mol^{-1}} \tag{1}$$

$$\mathrm{HO^-_{(solv.)} + [Al(Ohfip)_4]^-_{(solv.)} \rightarrow [Al(Ohfip)_4OH]^{2-}_{(solv.)}} \quad \Delta_r G°(2) = -62\ kJ\ mol^{-1} \tag{2}$$

$\Delta_r G°(1)$ implies equilibrium, and at standard conditions only one out of 10 molecules on the left reacts to the right. The solvated hydroxide ions thereby formed, immediately react with the $[Al(Ohfip)_4]^-$ anion according to (2) and give the dianion $[Al(Ohfip)_4OH]^{2-}$. Yet, this structure is not stable and easily loses solvated $[Ohfip]^-$ according to (3) as the more stable anion (cf. pK_a values: HO-hfip is the stronger acid than water [62]).

$$\mathrm{[Al(Ohfip)_4OH]^{2-}_{(solv.)} \rightarrow [Al(Ohfip)_3OH]^-_{(solv.)} + [Ohfip]^-_{(solv.)}} \quad \Delta_r G°(3) = -46\ kJ\ mol^{-1} \tag{3}$$

With 0.3 M solvated Mg^{2+} ions in the liquid electrolyte close by, the solvated $[Ohfip]^-$ anion will immediately undergo ion-pairing as in (4) to give the known [63] compound $Mg(Ohfip)_2$:

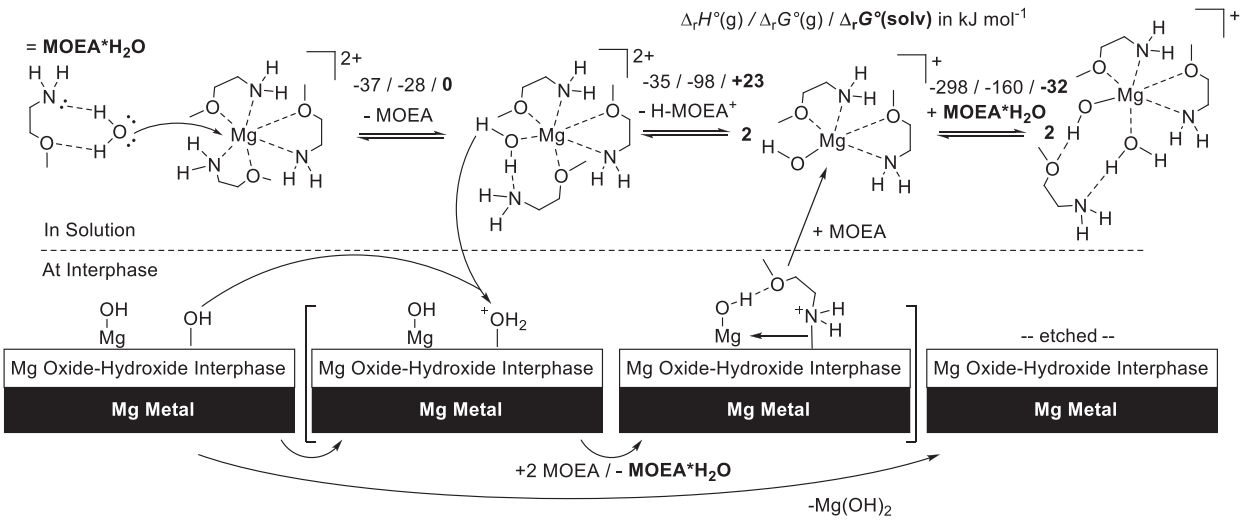
$$\mathrm{[Mg(MOEA)_3]^{2+}_{(solv.)} + 2\,[Ohfip]^-_{(solv.)} \rightarrow [Mg(MOEA)_2(Ohfip)_2]_{(solv.)} + MOEA} \quad \Delta_r G°(4) = -269\ kJ\ mol^{-1} \tag{4}$$

The solvated $[Al(Ohfip)_3OH]^-$ ion formed in Equation (3) will likely be in equilibrium with dimeric forms (5), e.g., mediated by ion-pairing with the Mg^{2+} ion in (6):

$$\mathrm{[Al(Ohfip)_3OH]^-_{(solv.)} \rightleftarrows [(hfipO)_3Al(\mu-OH)_2Al(Ohfip)_3]^{2-}_{(solv.)}} \quad \Delta_r G°(5) = +44\ kJ\ mol^{-1} \tag{5}$$

$$\mathrm{[(hfipO)_3Al(\mu-OH)_2Al(Ohfip)_3]^{2-}_{(solv.)} + [Mg(MOEA)_3]^{2+}_{(solv.)} \rightarrow [(hfipO)_6Al_2(OH)_2Mg(MOEA)]_{(solv.)} + 2MOEA_{(solv.)}} \quad \Delta_r G°(6) = -127\ kJ\ mol^{-1} \tag{6}$$

21983844, 2026, 59, Downloaded from https://advanced.onlinelibrary.wiley.com/doi/10.1002/advs.76897 by Toshihiko Mandai - National Institute For , Wiley Online Library on [23/10/2026]. See the Terms and Conditions (https://onlinelibrary.wiley.com/terms-and-conditions) on Wiley Online Library for rules of use; OA articles are governed by the applicable Creative Commons License



SCHEME 1 | Top, solution part: the four ions shown to be relevant for the solution chemistry; all others were too high in energy and hence not present in equilibrium. Bottom: Reaction at the Mg oxide-hydroxide interphase. The rather reactive $[Mg(MOEA)_3(OH_2)]^{2+}$ ion contains an (acidified, positively polarized) water molecule that may protonate a surface Mg-OH and thereby induce dissolution and etching of surface $Mg(OH)_2$ in the subsequent reaction sequence. The square brackets for the two middle species at the interphase indicate short-lived intermediates. Note that the entire scheme is stoichiometrically balanced.

Thermodynamically, the very exergonic reaction (6) will remove the dianion from the left side of the endergonic reaction (5). Overall, the sequence (1) to (6) implies that the pentacoordinate aluminate (Al_{CN5}) observed by NMR-spectroscopy is the Mg^{2+} complex of the dianion $[(hfipO)_3Al(\mu\text{-}OH)_2Al(Ohfip)_3]^{2-}$ and the second Ohfip-containing compound is the long-known $Mg(Ohfip)_2$.

Now we need to address the question as to why the hydroxylation stops at about 20% conversion of $[Al(Ohfip)_4]^-$ to the Mg^{2+} complex of $[(hfipO)_3Al(\mu\text{-}OH)_2Al(Ohfip)_3]^{2-}$. Hence, if we start in (1) with 2280 ppm water (=0.12 mol dm^{-3}), this should generate with $K(1) = 0.1$ only a small amount of hydroxide (0.006 mol dm^{-3}). In a 0.3 mol dm^{-3} electrolyte, the $[Al(Ohfip)_4]^-$ concentration is 0.6 mol dm^{-3}. Experimentally, we have seen the hydroxylation of 20% of $[Al(Ohfip)_4]^-$, that would correspond to 0.12 mol dm^{-3}. With the exergonic reactions (2) (−62 kJ mol^{-1}) and the $[Ohfip]^-$ scavenging by Mg^{2+} in (4) (−269 kJ mol^{-1}), the solvated $HO^-_{(solv.)}$ is withdrawn from (1) and yields the hydroxylated aluminate dianion. Apparently, and from the experiments described above, the formation of the hydroxylated aluminate dianion levels off at 0.12 mol dm^{-3} concentration. This may occur, when either all water is consumed or the reaction levels off due to the strong increase of the concentration of the cation $[H_2O{\bullet\bullet\bullet}H\text{-}MEOA]^+$ that has to form concomitantly with hydroxide in (1) and which increases the chemical potential in the system and stops further hydroxylation.

The analysis of the hydroxylation of the $[Al(Ohfip)_4]^-$ anion in the G2-MOEA system revealed that hydroxide ions are present in the electrolyte system. A broad evaluation of the structure and energetics of solvated $[Mg(OH)]^+$ or $[Mg(OH)_2]$ species was performed, that also did include water complexes of Mg compounds. Out of the investigation, the four ions shown on the top of Scheme 1 below were found to be relevant in the $Mg[Al(Ohfip)_4]_2$/MOEA solution; all others were too high in energy and hence not present in equilibrium. In the subsequent reactions, shown below at the Mg oxide-hydroxide interphase, now a surface $Mg(OH)_2$ may be solubilized by one reactive $[Mg(MOEA)_3(OH_2)]^{2+}$ ion in the form of two solvated $[Mg(OH)]^+$ complexes via the ammonium-assisted solubilization mechanism [64] – one emerging from the solution and one emerging from the surface-species. Hence, the high available concentration of $[Mg(MOEA)_3]^{2+}$ ions quickly removes the surface $Mg(OH)_2$ interphase as observed in the experiment. A substantial stability of amines against an electron also renders absence of MOEA decomposition during etching process very likely (cf. Scheme S5) [54, 65, 66].

The main difference between the $[Al(Ohfip)_4]^-$ and the $[TfO]^-$ electrolytes is the majority species in solution. While in the $[Al(Ohfip)_4]^-$-based, the reactive $[Mg(MOEA)_3]^{2+}$ ion is the majority species, in the $[TfO]^-$ electrolyte the ion-paired and H-bonded solvated $[Mg(TfO)_2]$ is the majority ion. As mentioned earlier, removal of the coordinated $[TfO]^-$ ions to give the $[Mg(MOEA)_3]^{2+}$ ion as found in the $[Al(Ohfip)_4]^-$ electrolyte, is a highly endergonic process. Hence, one expects the solvated $[Mg(TfO)_2]$ to be too unreactive, to activate and to etch the Mg oxide-hydroxide interphase. Moreover, $[TfO]^-$ is well known for its stability against hydrolysis [67]. The ^{19}F NMR spectra of the $Mg[TfO]_2$-based electrolytes clearly exclude the possibility of $[TfO]^-$ decomposition induced by trace water (Figure S18). All investigations into the structure and energetics of this process, the formation of water or hydroxide complexes, gave high energy species with the exception of one water adduct, but absolutely no hydroxide complex. These are at least 128 kJ mol^{-1} endergonic and not available for any surface modification. Overall, the Mg-coordination of the $[TfO]^-$ ion in the electrolytes lowers the reactivity so strongly that it can no longer serve to clean the surface. For full details, see the deposited sequence of reactions assessed in the §2.3 ESI. The presence of an appreciable amount of hydroxide ions in moist amine solvents also accounts for the relatively inferior Mg plating/stripping performance of the $Mg[TFSA]_2$-based amine-integrated systems compared to the

21983844, 2026, 59, Downloaded from https://advanced.onlinelibrary.wiley.com/doi/10.1002/advs.76897 by Toshihiko Mandai - National Institute For , Wiley Online Library on [23/10/2026]. See the Terms and Conditions (https://onlinelibrary.wiley.com/terms-and-conditions) on Wiley Online Library for rules of use; OA articles are governed by the applicable Creative Commons License

$Mg[TfO]_2$-based [22, 25], due to the limited stability of $[TFSA]^-$ under highly basic conditions [68].

Overall, the dynamic failure mechanism of the WCA-system is most likely driven by the MOEA-mediated and trace-water-driven hydroxylation of $[Al(Ohfip)_4]^-$, followed by inhomogeneous passivation and eventual localized utilization. Observation of negligible signals of fluorine- and nitrogen-containing species in the XPS spectra of the Mg metal soaked in the $Mg[Al(Ohfip)_4]_2$/G2-MOEA (Figure 3d) implies that the hydroxylation reaction byproducts, the Mg^{2+} complex with the dianion $[(hfipO)_6Al_2(OH)_2Mg(MOEA)]$ and $[Mg(MOEA)_2(Ohfip)_2]$, might be stable against initial, etched Mg metal. The electrochemical processes, however, promote decomposition of the accumulated byproducts on fresh Mg surfaces exposed through electrochemistry, eventually leading to the resistive interlayer formation. The suggestion of electrochemistry-promoted decomposition of byproducts is in good agreement with the XPS spectra of the cycled Mg electrodes, where the surface composition was rich in nitrogen and fluorine species (Figure S19). A relatively thick layer of highly amorphous decomposition products for the cycled Mg electrodes in $Mg[Al(Ohfip)_4]_2$/G2-MOEA also supports the instability of the byproducts against a fresh Mg surface (Figure 2c–g). Moreover, as the stripping of bulk metal preferentially takes place at the dislocation and/or grain boundary [69–71], the resulting resistive layer would be spatially inhomogeneous. The spatial inhomogeneity in the surface resistance will cause the uneven, localized utilization of Mg metal, ultimately leading to short-circuiting events at the early stage of cycling. These sequential interfacial processes are likely responsible to the complicated surface chemistry and particularly inferior electrochemical performance in the $Mg[Al(Ohfip)_4]_2$/G2-MOEA electrolyte (Figure 1a). Note that the equilibrium products between MOEA and H_2O initiate the above dynamic failure in composition, interface, and consequent electrochemistry. As the dynamic desolvation process at the interface does not directly correlate to the above interfacial decomposition processes, current densities for the galvanostatic cycling measurements have a minor impact on the long-term cycling stability (Figure S20). On the other hand, the failure of Mg plating/stripping in $Mg[B(Ohfip)_4]_2$/G2-MOEA (Figure S5) would likely be induced by different mechanisms as the *sp*3 boron center is not capable to accept additional coordination by OH^- due to its elemental characteristics. The ^1H, ^{11}B, and ^{19}F NMR spectra indeed corroborated the substantial stability of $[B(Ohfip)_4]^-$ even in the presence of hydroxide ions (Figure S21). As $[B(Ohfip)_4]^-$ gradually undergoes hydrolysis by water contamination [72], the decomposition of $[B(Ohfip)_4]^-$ causes impedance growth at a later stage and a short eventually.

It should be emphasized here that the above scenario, especially in the $Mg[Al(Ohfip)_4]_2$/G2-MOEA electrolyte, are evidently induced by water-contaminated MOEA; hence, a completely different picture in solution and at the interface can be anticipated for the water-free system. Nevertheless, due to the intrinsic characteristics of primary and secondary amines to form H-bonding with water molecules, complete dehydration of MOEA is unfeasible in practical as shown also by our rigorous drying conditions that could not remove the trace water to the desired low ppm level. Moreover, water contamination from other battery components, such as composite positive electrodes, separators, negative electrodes, tub, and casing, is inevitable in practical battery fabrication from a process perspective. Furthermore, side-reactions during battery operation can also potentially result in the generation of water molecules in the end [73, 74]. Since hydroxylation of $[Al(Ohfip)_4]^-$ is thermodynamically favorable, the following fluctuation of the Mg-electrolyte interface is also unavoidable once the electrolyte gets water contamination through various undesired events. Therefore, although investigation of the water-free systems will give distinct and valuable insights into the compositional and interfacial chemistries, electrolytes based on hydroxide-accepting WCAs with amine solvents are somehow inappropriate to practical battery applications and may reveal surprises with the capacity to donate hydroxide ions along the acid-base equilibrium. Hence, such failure mechanism – reported here for the first time for battery electrolytes – need to be considered in RMMB and all other battery systems, given that Brønsted basic solvents with amine functions are used.

2.4 | Full-Cell Performance and Complex Dilemma

As demonstrated above, no synergistic effect was observed from combining the two concepts—WCA-based Mg salts and alkoxyalkylamines—in RMMB electrolytes. Alkoxyalkylamines preferentially coordinate with coordinating and H-bonding anion-based Mg salts such as $Mg[TfO]_2$, leading to excellent electrochemical Mg plating/stripping performance in the $Mg[TfO]_2$/G2-MOEA electrolyte. Although these outstanding characteristics appear promising for practical applications, the reality is less favorable because this electrolyte exhibits serious drawbacks at the positive electrode side. Preliminary discharge–charge tests employing Chevrel phase Mo_6S_8 were successful while those employing high-voltage layered iron vanadate $FeV_3O_9{\bullet}1.1H_2O$ (FeVO) failed to exhibit reversible cycling with the $Mg[TfO]_2$/G2-MOEA electrolyte (Figure 5). In contrast, the MOEA-free simple ethereal electrolytes based on $Mg[Al(Ohfip)_4]_2$ exhibit good compatibility even with FeVO electrodes. The linear sweep voltammograms clearly reveal the inferior anodic stability of amine-containing electrolytes, regardless of the conductive salt used (Figure S22). A noticeable current increase due to electrolyte oxidation was observed at approximately 2.0 V vs. Mg, which is out of the voltage windows for operating high-voltage positive electrode materials. Moreover, $[TfO]^-$ is known to be highly corrosive toward Al current collectors, even at relatively low potentials [75]. This characteristic was also confirmed in the present study through chronoamperometric measurements and subsequent SEM observations (Figure S22). The intrinsically poor oxidation stability of amine solvents and strong corrosiveness of $[TfO]^-$ anions jointly contributed to the failure of cycling with FeVO. These background knowledge of the intrinsic physicochemical characteristics of every $Mg[TfO]_2$-amine system are particularly important in designing high-performance electrolytes that are compatible with both Mg negative and high-voltage positive electrodes for the future development.

Considering all experimental and calculational results collectively, the relationship between compositional and interfacial chemistry is summarized in Figure 6. The mechanistic investigation based on NMR spectroscopy, combined with quantum

21983844, 2026, 59, Downloaded from https://advanced.onlinelibrary.wiley.com/doi/10.1002/advs.76897 by Toshihiko Mandai - National Institute For , Wiley Online Library on [23/10/2026]. See the Terms and Conditions (https://onlinelibrary.wiley.com/terms-and-conditions) on Wiley Online Library for rules of use; OA articles are governed by the applicable Creative Commons License

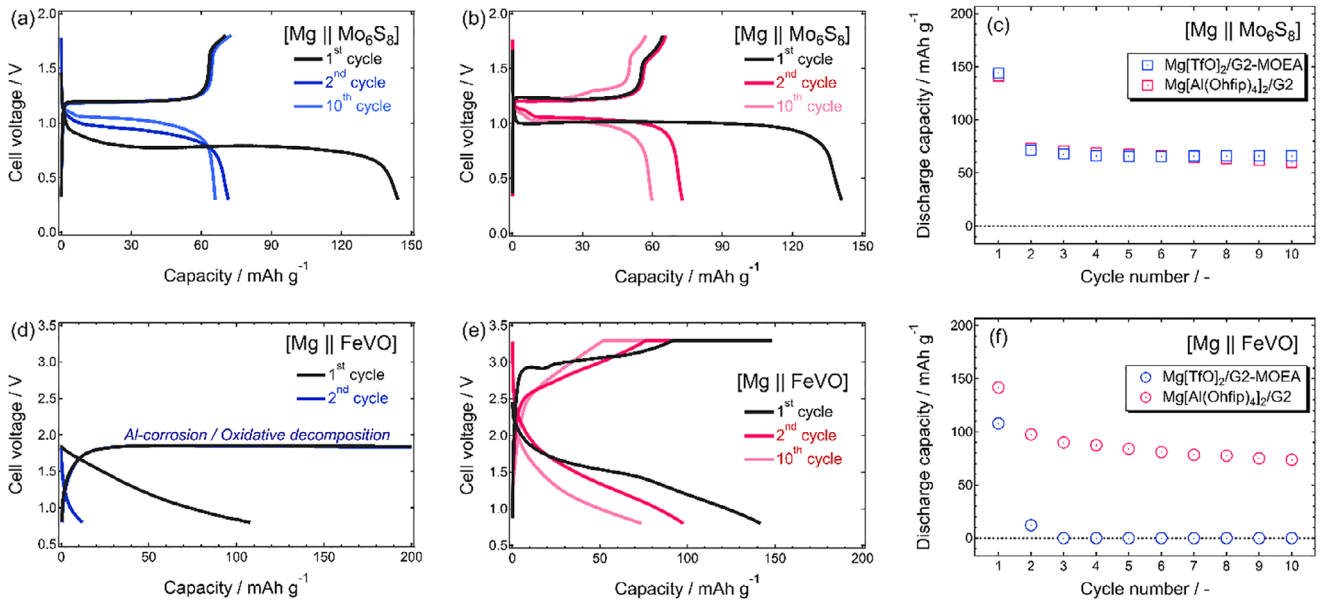


FIGURE 5 | Discharge-charge profiles of (a, b) [Mg || Mo_6S_8] and (d, e) [Mg || FeVO] cells using (a, d) $Mg[TfO]_2$/G2-MOEA and (b, e) $Mg[Al(Ohfip)_4]_2$/G2 as electrolytes. Discharge capacity retention of (c) [Mg || Mo_6S_8] and (f) [Mg || FeVO] cells.

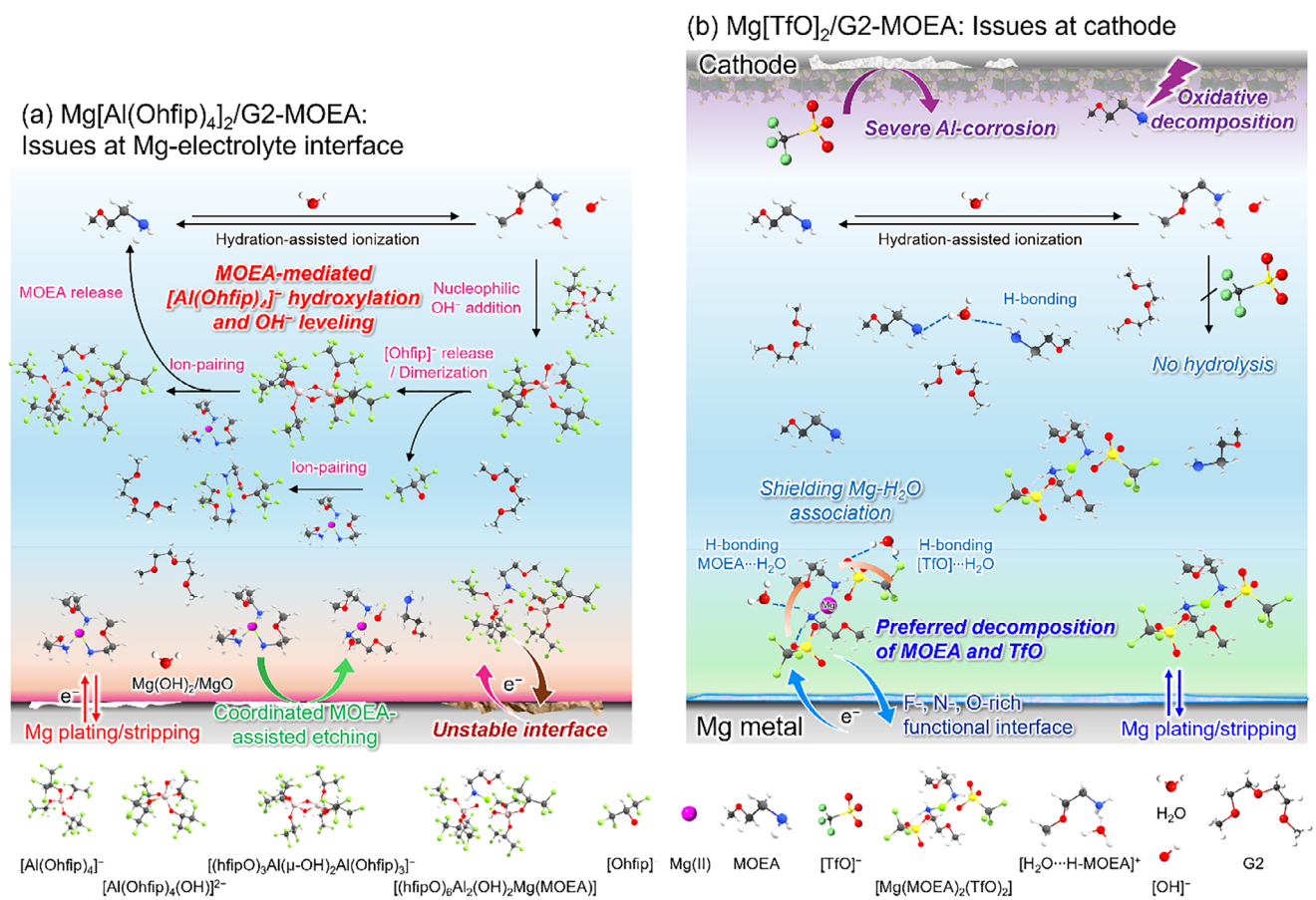


FIGURE 6 | Schematic illustration of the relationship between compositional and interfacial chemistries in (a) $Mg[Al(Ohfip)_4]_2$/G2-MOEA and (b) $Mg[TfO]_2$/G2-MOEA electrolytes.

21983844, 2026, 59, Downloaded from https://advanced.onlinelibrary.wiley.com/doi/10.1002/advs.76897 by Toshihiko Mandai - National Institute For , Wiley Online Library on [23/10/2026]. See the Terms and Conditions (https://onlinelibrary.wiley.com/terms-and-conditions) on Wiley Online Library for rules of use; OA articles are governed by the applicable Creative Commons License

chemical calculations and vibrational analysis, revealed the MOEA-mediated and trace-water-driven partial hydroxylation of $[Al(Ohfip)_4]^-$ (Figure 6a). The rather reactive $[Mg(MOEA)_3]^{2+}$ and $[Mg(MOEA)_3(OH_2)]^{2+}$ ions present would dissolve the surface $Mg(OH)_2$ via the ammonium-assisted solubilization mechanism [64]. Consumption of water impurity by the partial hydroxylation and $[Mg(MOEA)_3]^{2+}$-mediated etching effect may jointly contribute to forming less insulative oxygen-rich interface, which likely accounts for the exceptionally low interfacial resistance (Figure 1d). However, the hydroxylation of the anion and the resulting complicated cation-anion complex formation would in turn result at later stages in an unstable interface for the electrochemical Mg plating/stripping reactions (Figure 1a). For the $Mg[TfO]_2$-based electrolyte, Mg^{2+} is coordinated by the strongly associative $[TfO]^-$ ion and MOEA in the solutions. The reactivity of trace water molecules is suppressed through H-bonding with MOEA. The strongly solvated $[TfO]^-$ and MOEA species in the primary solvation sheath are prone to reduction at the interface. The mutual cation-anion, solvent–anion, and solvent–water interactions and the resulting functional interphase may collectively contribute to the stabilization of the interface and remarkable electrochemical performance for the $Mg[TfO]_2$/G2-MOEA electrolyte (Figure 1b). Unfortunately, its limited anodic stability and strong corrosiveness toward the Al current collector in turn hinder its application in practical RMMBs (Figure 6b). Therefore, the development of electrolyte systems still faces an unresolved fundamental dilemma: materials that provide excellent compatibility at one electrode often compromise the performance at the other. Rational, multilateral design strategies are urgently needed to develop high-performance RMMBs capable of overcoming these complex trade-offs.

3 | Conclusions

The development of electrolyte materials that meet the requirements of both negative and positive electrode materials remains a long-standing challenge in RMMB research. Two recent groundbreaking concepts—the adoption of weakly coordinating anions (WCAs) and the use of alkoxyalkylamine-based solvents in electrolyte formulations—have individually demonstrated excellent compatibility, particularly with Mg negative electrodes. However, combining these two approaches has led to unexpectedly poor electrochemical performance. The electrolyte formulation with rather associative anions, in turn, exhibits remarkably favorable Mg plating/stripping performance. Comprehensive electrochemical, compositional, physical, spectroscopic, and computational analyses revealed a counter-anion-dependent solvation structure. In the $Mg[Al(Ohfip)_4]_2$/G2-MOEA system, Mg^{2+} is primarily surrounded solely by chelating MOEA solvent molecules, whereas in the $Mg[TfO]_2$-based counterpart, both $[TfO]^-$ and MOEA participate in coordination of Mg^{2+}, and MOEA molecules are also bound to coordinated $[TfO]^-$ via H-bonding, thereby forming a multi-compositional solvation sheath. Such distinct solvation environments are likely responsible for the observed interfacial compositions and consequent electrochemical characteristics. Moreover, detailed spectroscopic analyses combined with quantum chemical calculations revealed an unprecedented susceptibility of $[Al(Ohfip)_4]^-$ to trace amounts of water in the presence of MOEA. The MOEA-mediated partial hydroxylation of $[Al(Ohfip)_4]^-$ combined with a peculiar etching effect effectively scavenges detrimental trace water and removes insulative $Mg(OH)_2$ from the initial Mg-interface, thereby leading to the formation of a less-insulative interphase. Yet, the hydroxylation also results in the formation of large cation-anion aggregate complexes, which in turn causes undesirable electrochemical performance. In contrast, the hydrophobic and highly associative nature of $Mg[TfO]_2$ prevents water molecules from approaching the inner solvation sheath. The passivation of Mg metal by trace water is likely suppressed through the formation of a fluorine- and nitrogen-rich functional interphase derived from $[TfO]^-$ and MOEA, as well as by the restriction of water reactivity via H-bonding with MOEA and $[TfO]^-$.

Despite the excellent electrochemical Mg plating/stripping behavior of the $Mg[TfO]_2$/G2-MOEA electrolyte, its limited anodic stability and strong corrosiveness toward the Al current collector hinder its application in practical RMMBs. Regarding compatibility with positive electrodes, conventional ethereal electrolytes based on WCAs exhibit clear advantages over $[TfO]^-$–amine systems, although their Mg plating/stripping performance remains insufficient for practical battery implementation. With respect to compositional engineering, regulating the interfacial stability of the WCA-salt ether systems by rational halide-free additives would be the most straightforward approaches to satisfy the requirements from both positive and negative electrode sides. Ishfaq et al., recently demonstrated significantly enhanced performance of the benchmarking $Mg[Al(Ohfip)_4]_2$/G2 electrolyte upon the integration of a well-controlled amount of fluorinated cyclic ether [76]. Our group also developed the mixed-coordination electrolyte combined with a fluorinated molecular additive which promotes anion- and additive-derived favorable interphase formations and enhances cycling stability in high-voltage RMBs [77]. As the integration of large quantity of non-coordinating diluents like fluorinated ether in the ethereal electrolytes is detrimental for Mg plating/stripping performance [20, 21], the dosage needs to be adjusted appropriately. In addition to the above compositional approaches, Mg^{2+}-conductive alloy-derived artificial interphases have attracted significant attention owing to their favorable characteristics [41, 78, 79]. Certain artificial interphase effectively regulates Mg^{2+}-ion flux at the electrode surface and promote interfacial kinetics, thereby improving overall battery performance. Since the development of electrolyte materials through the adoption of non-ethereal solvents remains challenging due to the limited compatibility of highly reductive Mg metal with organic compounds [30], combining advanced ethereal electrolyte solutions with functional interphases could pave the way toward realizing high-energy-density RMMBs.

Author Contributions

Toshihiko Mandai: Conceptualization, Data curation, Formal analysis, Funding acquisition, Investigation, Project administration, Resources, Validation, Writing – original draft, reviewing, and editing. **Antoine Barthélemy:** Quantum chemical calculations, Formal analysis, Validation, Writing – reviewing and editing. **Hendrik Koger:** Karl-Fischer titration, FT-IR measurements, Formal analysis, Resources, Validation, Writing – reviewing and editing. **Harald Scherer:** NMR measurements, Formal analysis, Validation, Writing – reviewing and editing. **Ingo Krossing:** Formal analysis, Validation, Writing – reviewing and editing.

21983844, 2026, 59, Downloaded from https://advanced.onlinelibrary.wiley.com/doi/10.1002/advs.76897 by Toshihiko Mandai - National Institute For , Wiley Online Library on [23/10/2026]. See the Terms and Conditions (https://onlinelibrary.wiley.com/terms-and-conditions) on Wiley Online Library for rules of use; OA articles are governed by the applicable Creative Commons License

Acknowledgements

This work was supported in part by the NEXT Center of Innovation Program (COI-NEXT; grant number JPMJPF2016) of the Japan Science and Technology Agency and KAKENHI (grant number JP26K01623) of the Japan Society for the Promotion of Science. Additionally, this work was supported by the Albert-Ludwigs-Universität Freiburg, by the state of Baden-Württemberg through bwHPC and the German Research Foundation (DFG) through grant number INST 40/467-1 and 575-1 FUGG (JUSTUS 1 and 2 cluster), the DFG project AMPERE (project number 441215516), the EU project HighMag (Grant agreement ID: 101202882), as well as the European Research Council's ERC Advanced Grant InnoChem (Grant agreement ID: 101052935). The authors acknowledge Ms. Watanabe, Ms. Oshida, and Mr. Shinoda for their assistance with microscopic observations. The XRD profiles, SEM images, XPS spectra, TOF-SIMS spectra, STEM images, EELS spectra, and electrochemical confocal microscopic analyses of Mg plating/stripping reactions were obtained using the facilities of Battery-PF at NIMS, Japan.

Conflicts of Interest

The authors declare no conflicts of interest.

Data Availability Statement

The data that support the findings of this study are available from the corresponding author upon reasonable request.

References

1. F. Degen, M. Winter, D. Bendig, and J. Tübke, "Energy Consumption of Current and Future Production of Lithium-Ion and Post Lithium-Ion Battery Cells," *Nature Energy* 8 (2023): 1284.

2. J. A. Blázquez, R. R. Maça, O. Leonet, et al., "A Practical Perspective on the Potential of Rechargeable Mg Batteries," *Energy & Environmental Science* 16 (2023): 1964.

3. D. Wang, Z. Zhang, Y. Hao, et al., "Challenges and Progress in Rechargeable Magnesium-Ion Batteries: Materials, Interfaces, and Devices," *Advanced Functional Materials* 34 (2024): 2410406.

4. I. M. Riddlestone, A. Kraft, J. Schaefer, and I. Krossing, "Taming the Cationic Beast: Novel Developments in the Synthesis and Application of Weakly Coordinating Anions," *Angewandte Chemie International Edition* 57 (2018): 13982.

5. A. Barthélemy, P. Dabringhaus, and E. Jacob, et al., *Comprehensive Inorganic Chemistry III* (Elsevier, 2023), 378–438.

6. O. Tutusaus, R. Mohtadi, T. S. Arthur, F. Mizuno, E. G. Nelson, and Y. V. Sevryugina, "An Efficient Halogen-Free Electrolyte for Use in Rechargeable Magnesium Batteries," *Angewandte Chemie International Edition* 54 (2015): 7900.

7. J. T. Herb, C. A. Nist-Lund, and C. B. Arnold, "A Fluorinated Alkoxyaluminate Electrolyte for Magnesium-Ion Batteries," *ACS Energy Letters* 1 (2016): 1227.

8. Z. Zhao-Karger, M. E. Gil Bardaji, O. Fuhr, and M. Fichtner, "A New Class of Non-Corrosive, Highly Efficient Electrolytes for Rechargeable Magnesium Batteries," *Journal of Materials Chemistry A* 5 (2017): 10815.

9. R. Jay, A. W. Tomich, J. Zhang, et al., "Comparative Study of $Mg(CB_{11}H_{12})_2$ and $Mg(TFSI)_2$ at the Magnesium/Electrolyte Interface," *ACS Applied Materials & Interfaces* 11 (2019): 11414.

10. N. T. Hahn, T. J. Seguin, K.-C. Lau, et al., "Enhanced Stability of the Carba-Closo-dodecaborate Anion for High Voltage Battery Electrolytes Through Rational Design," *Journal of the American Chemical Society* 140 (2018): 11076.

11. W. Ren, D. Wu, Y. NuLi, et al., "An Efficient Bulky $Mg[B(Otfe)_4]_2$ Electrolyte and Its Derivatively General Design Strategy for Rechargeable Magnesium Batteries," *ACS Energy Letters* 6 (2021): 3212.

12. S. Zhang, M. Cheng, P. Zhang, et al., "Insights Into the Stability of Magnesium Borate Salts for Rechargeable Magnesium Batteries From AIMD Simulations," *Chemical Communications* 58 (2022): 11969.

13. T. Mandai, "Critical Issues of Fluorinated Alkoxyborate-Based Electrolytes in Magnesium Battery Applications," *ACS Applied Materials & Interfaces* 12 (2020): 39135.

14. T. Mandai, Y. Youn, and Y. Tateyama, "Remarkable Electrochemical and Ion-Transport Characteristics of Magnesium-Fluorinated Alkoxyaluminate–Diglyme Electrolytes for Magnesium Batteries," *Materials Advances* 2 (2021): 6283.

15. P. Jankowski, Z. Li, Z. Zhao-Karger, et al., "Development of Magnesium Borate Electrolytes: Explaining the Success of $Mg[B(hfip)_4]_2$ Salt," *Energy Storage Materials* 45 (2022): 1133.

16. Z. Zhang, Z. Cui, L. Qiao, et al., "Novel Design Concepts of Efficient Mg-Ion Electrolytes Toward High-Performance Magnesium–Selenium and Magnesium–Sulfur Batteries," *Advanced Energy Materials* 7 (2017): 1602055.

17. X. Huang, S. Tan, J. Chen, et al., "Asymmetric $SO_3CF_3^-$-Grafted Boron-Center Anion Enables Boron-Containing Interphase for High-Performance Rechargeable Mg Batteries," *Advanced Functional Materials* 34 (2024): 2314146.

18. T. Pavčnik, M. Lozinšek, K. Pirnat, et al., "On the Practical Applications of the Magnesium Fluorinated Alkoxyaluminate Electrolyte in Mg Battery Cells," *ACS Applied Materials & Interfaces* 14 (2022): 26766.

19. S. Riedel, L. Wang, M. Fichtner, and Z. Zhao-Karger, "Recent Advances in Electrolytes for Magnesium Batteries: Bridging the gap Between Chemistry and Electrochemistry," *Chemistry – A European Journal* 30 (2024): 202402754.

20. T. Mandai, M. Yao, K. Sodeyama, A. Kagatsume, Y. Tateyama, and H. Imai, "Toward Improved Anodic Stability of Ether B ased Electrolytes for Rechargeable Magnesium Batteries," *Journal of Physical Chemistry C* 127 (2023): 10419.

21. N. T. Hahn, E. P. Kamphaus, Y. Chen, et al., "Magnesium Battery Electrolytes With Improved Oxidative Stability Enabled by Selective Solvation in Fluorinated Solvents," *ACS Applied Energy Materials* 6 (2023): 3264.

22. Z. Li, D. Nguyen, J. D. Bazak, et al., "Stable Cycling of Mg Metal Anodes by Regulating the Reactivity of Mg^{2+} Solvation Species," *Advanced Energy Materials* 14 (2024): 2301544.

23. J. Zhang, N. Yuan, J. Liu, et al., "Activation Mechanism of Conventional Electrolytes With Amine Solvents: Species Evolution and Hydride-Containing Interphase Formation," *Journal of Energy Chemistry* 98 (2024): 615.

24. J. Xiao, X. Zhang, H. Fan, et al., "Cosolvent-Assisted Formation of Charged Ion-Solvent Clusters and Solid Electrolyte Interphase for High-Performance Magnesium Metal Batteries," *Advanced Energy Materials* 12 (2022): 2202602.

25. D. Zhang, Y. Wang, Y. Yang, et al., "Constructing Efficient $Mg(CF_3SO_3)_2$ Electrolyte via Tailoring Solvation and Interface Chemistry for High-Performance Rechargeable Magnesium Batteries," *Advanced Energy Materials* 13 (2023): 2301795.

26. H. Fan, X. Zhang, J. Xiao, et al., "Tailoring Electrode–Electrolyte Interface Using an Electron-Deficient Borate-Based Additive in $MgTFSI_2$-$MgCl_2$/DME Electrolyte for Rechargeable Magnesium Batteries," *Energy & Environmental Materials* 7 (2024): 12792.

27. Z. Meng, Z. Li, L. Wang, et al., "Surface Engineering of a Mg Electrode via a New Additive to Reduce Overpotential," *ACS Applied Materials & Interfaces* 13 (2021): 37044.

28. T. Mandai, "Enhanced Reversibility of Mg Plating/Stripping via Solvation Sheath Regulation by a Multidentate Linear Oligoether," *Batteries & Supercaps* 8 (2025): e202500348.

21983844, 2026, 59, Downloaded from https://advanced.onlinelibrary.wiley.com/doi/10.1002/advs.76897 by Toshihiko Mandai - National Institute For , Wiley Online Library on [23/10/2026]. See the Terms and Conditions (https://onlinelibrary.wiley.com/terms-and-conditions) on Wiley Online Library for rules of use; OA articles are governed by the applicable Creative Commons License

29. S.-B. Son, T. Gao, S. P. Harvey, et al., "An Artificial Interphase Enables Reversible Magnesium Chemistry in Carbonate Electrolytes," *Nature Chemistry* 10 (2018): 532.

30. T. Mandai, "Mg Plating in Nonethereal Electrolyte Solutions: Fact or Misconception?," *ChemSusChem* 18 (2025): 202500418.

31. D. M. Overcash and F. C. Mathers, "The Electrodeposition of Magnesium," *Transactions of The Electrochemical Society* 64 (1933): 305.

32. S. Fan, G. M. Asselin, B. Pan, et al., "A Simple Halogen-Free Magnesium Electrolyte for Reversible Magnesium Deposition Through Cosolvent Assistance," *ACS Applied Materials & Interfaces* 12 (2020): 10252.

33. S. Hou, X. Ji, K. Gaskell, et al., "Solvation Sheath Reorganization Enables Divalent Metal Batteries With Fast Interfacial Charge Transfer Kinetics," *Science* 374 (2021): 172.

34. Y. Du, Y. Chen, S. Tan, et al., "Strong Solvent Coordination Effect Inducing Gradient Solid-Electrolyte-Interphase Formation for Highly Efficient Mg Plating/Stripping," *Energy Storage Materials* 62 (2023): 102939.

35. F. Wang, H. Hua, D. Wu, et al., "Solvent Molecule Design Enables Excellent Charge Transfer Kinetics for a Magnesium Metal Anode," *ACS Energy Letters* 8 (2023): 780.

36. M. Wang, W. Sun, K. Zhang, et al., "Synergy Between the Coordination and Trace Ionization of Co-Solvents Enables Reversible Magnesium Electroplating/Stripping Behavior," *Energy & Environmental Science* 17 (2024): 630.

37. Z. Yang, J. Zhang, X. Du, et al., "Evolution and Underlying Mechanisms of MgH_2 in Amine-Based Electrolytes for Magnesium Metal Batteries," *Energy Storage Materials* 84 (2026): 104842.

38. X. Liu, A. Du, Z. Guo, et al., "Uneven Stripping Behavior, an Unheeded Killer of Mg Anodes," *Advanced Materials* 34 (2022): 2201886.

39. J. Eaves-Rathert, K. Moyer, M. Zohair, and C. L. Pint, "Kinetic- Versus Diffusion-Driven Three-Dimensional Growth in Magnesium Metal Battery Anodes," *Joule* 4 (2020): 1324.

40. T. Mandai and H. Somekawa, "Ultrathin Magnesium Metal Anode—An Essential Component for High-Energy-Density Magnesium Battery," *Batteries & Supercaps* 5 (2022): e202200153.

41. T. Mandai, U. Tanaka, and M. Watanabe, "Mg–Zn–Cl-Integrated Functional Interface for Enhancing the Cycle Life of Mg Electrodes," *Energy Storage Materials* 67 (2024): 103302.

42. M. Matsui, "Study on Electrochemically Deposited Mg Metal," *Journal of Power Sources* 196 (2011): 7048.

43. C. Li, W. Sun, H. Zhou, et al., "Dendritic Magnesium Formation in Conventional Electrolytes: Local Adsorption of Amine Solvents at Inner Helmholtz Plane Matters," *Advanced Functional Materials* 35 (2025): 2417287.

44. S. J. Pike, J. J. Hutchinson, and C. A. Hunter, "H-Bond Acceptor Parameters for Anions," *Journal of the American Chemical Society* 139 (2017): 6700.

45. C. M. Burba, N. M. Rocher, R. Frech, and D. R. Powell, "Cation-Anion Interactions in 1-ethyl-3-Methylimidazolium Trifluoromethanesulfonate-Based Ionic Liquid Electrolytes," *Journal of Physical Chemistry B* 112 (2008): 2991.

46. R. Frech and W. Huang, "Anion-Solvent and Anion-Cation Interactions in Lithium and Tetrabutylammonium Trifluoromethanesulfonate Solutions," *Journal of Solution Chemistry* 23 (1994): 469.

47. C. M. Burba, N. M. Rocher, and R. Frech, "Hydrogen-Bonding and Ion−Ion Interactions in Solutions of Triflic Acid and 1-Ethyl-3-Methylimidazolium Triflate," *Journal of Physical Chemistry B* 113 (2009): 11453.

48. W. Huang, R. A. Wheeler, and R. Frech, "Vibrational Spectroscopic and Ab Initio Molecular Orbital Studies of the Normal and ^{13}C-Labeled Trifluoromethanesulfonate Anion," *Spectrochimica Acta* 50A (1994): 985.

49. K. Hoshi, T. Chiba, J. Sato, et al., "Purification of Perovskite Quantum Dots Using Low-Dielectric-Constant Washing Solvent "Diglyme" for Highly Efficient Light-Emitting Devices," *ACS Applied Materials & Interfaces* 10 (2018): 24607.

50. S. A. Skaanvik, J. D. Henderson, J. J. Noël, and M. C. Biesinger, "Speciation of Magnesium Surfaces by X-Ray Photoelectron Spectroscopy (XPS)," *Surface and Interface Analysis* 57 (2025): 717.

51. X. Xie, N. J. Leon, D. W. Small, E. W. C. Spotte-Smith, C. Liao, and K. A. Persson, "Reductive Decomposition Kinetics and Thermodynamics That Govern the Design of Fluorinated Alkoxyaluminate/Borate Salts for Mg-Ion and Ca-Ion Batteries," *Journal of Physical Chemistry C* 126 (2022): 20773.

52. N. N. Rajput, X. Qu, N. Sa, A. K. Burrell, and K. A. Persson, "The Coupling Between Stability and Ion Pair Formation in Magnesium Electrolytes From First-Principles Quantum Mechanics and Classical Molecular Dynamics," *Journal of the American Chemical Society* 137 (2015): 3411.

53. J. Burrows, S. Kamo, and K. Koide, "Scalable Birch Reduction With Lithium and Ethylenediamine in Tetrahydrofuran," *Science* 374 (2021): 741.

54. A. G. Seel, H. Swan, D. T. Bowron, et al., "Electron Solvation and the Unique Liquid Structure of a Mixed-Amine Expanded Metal: The Saturated Li–NH_3–$MeNH_2$ System," *Angewandte Chemie International Edition* 56 (2017): 1561.

55. Hydranal Laboratory Report L288, Water determination in nitrogen bases, http://lab.solstice.com/en/resources/hydranal-lab-reports/water-determination-in-nitrogen-bases. Accessed on 3rd of June, 2026.

56. Z. Zhao, D. Xiao, K. Chen, et al., "Nature of Five-Coordinated Al in γ-Al_2O_3 Revealed by Ultrahigh-Field ^{27}Al MAS NMR," *ACS Central Science* 8 (2022): 795.

57. M. Gonsior, I. Krossing, and N. Mitzel, "A Thallium Coated Dianion: Trigonal Bipyramidal $[F_2Al(OR)_3]^{2-}$ Coordinated to Three Tl^+ Cations in the Ion Pair $[Tl_3F_2Al(OR)_3]^+[Al(OR)_4]^-$ [R = $CH(CF_3)_2$]," *Zeitschrift für anorganische und allgemeine Chemie* 628 (2002): 1821.

58. A. Kraft, J. Possart, H. Scherer, J. Beck, D. Himmel, and I. Krossing, "The $Al(OR^F)_3/H_2O$/Phosphane [R^F = $C(CF_3)_3$] System—Protonation of Phosphanes and Absolute Brønsted Acidity," *European Journal of Inorganic Chemistry* 2013 (2013): 3054.

59. M. Lozinšek, T. Pavčnik, and J. Bitenc, "Bis(dimethoxyethane-1κ^2O,O′)pentakis(1,1,1,3,3,3-hexafluoropropan-2-olato)-2κ^3O,3κ^2O-μ-hydroxido-1:3κ^2O-μ_3-oxido-1:2:3κ^3O-magnesiumdialuminium," *IUCrData* 8 (2023): x230716.

60. K. Tang, A. Du, X. Du, et al., "A Novel Regulation Strategy of Solid Electrolyte Interphase Based on Anion-Solvent Coordination for Magnesium Metal Anode," *Small* 16 (2020): 2005424.

61. P. Love, R. B. Cohen, and R. W. Taft, "Polar Substituent Effects In Gas-Phase Lewis Acid-Base Equilibriums. I. Insrinsic Basicity of Amines," *Journal of the American Chemical Society* 90 (1968): 2455.

62. I. Colomer, A. E. R. Chamberlain, M. B. Haughey, and T. J. Donohoe, "Hexafluoroisopropanol as a Highly Versatile Solvent," *Nature Reviews Chemistry* 1 (2017): 0088.

63. J. Long, Y. Liu, Z. He, et al., "Redesigning Solvation Structure Toward Passivation-Free Magnesium Metal Batteries," *ACS Nano* 18 (2024): 15239.

64. A. F. Holleman, E. Wiberg, and N. Wiberg, *Lehrbuch der Anorganischen Chemie* (Auflage. Walter de Gruyter, 2007), 1230–1231, ISBN 978-3-11-017770-1.

65. P. P. Edwards, H. B. Gray, M. T. J. Lodge, and R. J. P. Williams, "Electron Transfer and Electronic Conduction Through an Intervening Medium," *Angewandte Chemie International Edition* 47 (2008): 6758.

66. V. V. Chaban and O. V. Prezhdo, "Electron Solvation in Liquid Ammonia: Lithium, Sodium, Magnesium, and Calcium as Electron Sources," *Journal of Physical Chemistry B* 120 (2016): 2500.

21983844, 2026, 59, Downloaded from https://advanced.onlinelibrary.wiley.com/doi/10.1002/advs.76897 by Toshihiko Mandai - National Institute For , Wiley Online Library on [23/10/2026]. See the Terms and Conditions (https://onlinelibrary.wiley.com/terms-and-conditions) on Wiley Online Library for rules of use; OA articles are governed by the applicable Creative Commons License

67. G. R. Pastel, M. S. Ding, T. P. Pollard, O. Borodin, M. Schroeder, and K. Xu, "Cation-Dependent Solvation Behavior of Aqueous Triflate Electrolytes," *ACS Electrochemistry* 1 (2025): 486.

68. A. France-Lanord, F. Pietrucci, A. M. Saitta, J.-M. Tarascon, A. Grimaud, and M. Salanne, "Chemical Decomposition of the TFSI Anion Under Aqueous Basic Conditions," *PRX Energy* 1 (2022): 013005.

69. T. Mandai and H. Somekawa, "Metallurgical Approach to Enhance the Electrochemical Activity of Magnesium Anodes for Magnesium Rechargeable Batteries," *Chemical Communications* 56 (2020): 12122.

70. C. Xie, S. Liu, Z. Yang, et al., "Discovering the Intrinsic Causes of Dendrite Formation in Zinc Metal Anodes: Lattice Defects and Residual Stress," *Angewandte Chemie International Edition* 62 (2023): e202218612.

71. S. Wu, Z. Hu, P. He, L. Ren, J. Huang, and J. Luo, "Crystallographic Engineering of Zn Anodes for Aqueous Batteries," *eScience* 3 (2023): 100120.

72. J. Luo, Y. Bi, L. Zhang, X. Zhang, and T. L. Liu, "A Stable, Non-Corrosive Perfluorinated Pinacolatoborate Mg Electrolyte for Rechargeable Mg Batteries," *Angewandte Chemie International Edition* 58 (2019): 6967.

73. J. S. Edge, S. O'Kane, R. Prosser, et al., "Lithium Ion Battery Degradation: What You Need to Know," *Physical Chemistry Chemical Physics* 23 (2021): 8200.

74. Y. Gao, H. Noguchi, and K. Uosaki, "Online Real-Time Detection of the Degradation Products of Lithium Oxygen Batteries," *ACS Energy Letters* 8 (2023): 1811.

75. S. S. Zhang and T. R. Jow, "Aluminum Corrosion in Electrolyte of Li-Ion Battery," *Journal of Power Sources* 109 (2002): 458.

76. H. A. Ishfaq, A. Marojević, C. C. Cardona, et al., "Stabilizing Magnesium Anodes in Rechargeable Magnesium Batteries via Fluorinated Cyclic Ether Electrolyte Additive," *Advanced Energy Materials* 16 (2026): e06415.

77. D. Setiawan and T. Mandai, "Mixed-Coordination Electrolytes With Molecular Additives for Robust Interphases in High-Voltage Rechargeable Magnesium Batteries," *Advanced Science* (2026): e75749, https://doi.org/10.1002/advs.75749.

78. C. Pechberty, A. Hagopian, J.-B. Ledeuil, et al., "Alloying Electrode Coatings Towards Better Magnesium Batteries," *Journal of Materials Chemistry A* 10 (2022): 12104.

79. X. Hou, J. Guan, B. Wu, et al., "Bismuth/Tin-Based Artificial Interface for Overcoming the Anode Passivation of Rechargeable Magnesium Batteries," *Chemical Communications* 61 (2025): 12546.

Supporting Information

Additional supporting information can be found online in the Supporting Information section.

Supporting File 1: advs76897-sup-0001-SuppMat.docx.

Supporting File 2: advs76897-sup-0002-SuppVideos.zip.

21983844, 2026, 59, Downloaded from https://advanced.onlinelibrary.wiley.com/doi/10.1002/advs.76897 by Toshihiko Mandai - National Institute For , Wiley Online Library on [23/10/2026]. See the Terms and Conditions (https://onlinelibrary.wiley.com/terms-and-conditions) on Wiley Online Library for rules of use; OA articles are governed by the applicable Creative Commons License